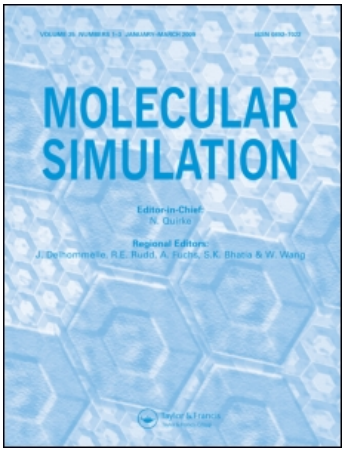

Molecular Simulation
Publication details, including instructions for authors and subscription information:
http://www.informaworld.com/smpp/title~content=t713644482

Grand Canonical Ensemble Monte Carlo Simulations of Donnan Potentials, Nonelectroneutrality, Activity Coefficients and Excess Energy in Spherical Charged or Uncharged Pores with Restricted Primitive Model Electrolytes

Sergio Roberto Rivera[ab]; Torben Smith Søsrensen[ab]
[a] Institute of Physical Chemistry, Technical University of Denmark, Lyngby, Denmark [b] Institute of Physical Chemistry and Center for Modelling, Nonlinear Systems Dynamics and Irreversible Thermodynamics, Technical University of Denmark, Vanløse, Denmark

To cite this Article Rivera, Sergio Roberto and Søsrensen, Torben Smith(1994) 'Grand Canonical Ensemble Monte Carlo Simulations of Donnan Potentials, Nonelectroneutrality, Activity Coefficients and Excess Energy in Spherical Charged or Uncharged Pores with Restricted Primitive Model Electrolytes', Molecular Simulation, 13: 2, 115 — 160
To link to this Article: DOI: 10.1080/08927029408021978
URL: http://dx.doi.org/10.1080/08927029408021978

Molecular Simulation, 1994, Vol. 13, pp. 115–160
Reprints available directly from the publisher
Photocopying permitted by license only Printed in Malaysia

GRAND CANONICAL ENSEMBLE MONTE CARLO SIMULATIONS OF DONNAN POTENTIALS, NONELECTRONEUTRALITY, ACTIVITY COEFFICIENTS AND EXCESS ENERGY IN SPHERICAL CHARGED OR UNCHARGED PORES WITH RESTRICTED PRIMITIVE MODEL ELECTROLYTES

SERGIO ROBERTO RIVERA and TORBEN SMITH SØRENSEN*

Institute of Physical Chemistry, Technical University of Denmark, Building 206, DK2800 Lyngby, Denmark and Institute of Physical Chemistry and Center for Modelling, Nonlinear Systems Dynamics and Irreversible Thermodynamics, Technical University of Denmark, Nørager Plads 3, DK2720 Vanløse, Denmark

(Received November, 1993, accepted November, 1993)

A great number of Grand Canonical Ensemble simulations have been performed for restricted primitive model electrolytes in spherical hard-wall pores with the same dielectric permittivity in the pores and in the wall. The pores have a continuously distributed surface charge from 0 to 10 elementary charges and radii from 1 to 35 ionic diameters. When a pore is in equilibrium with an outside bulk solution, it acquires in the average a certain deviation from electroneutrality (spontaneous electrification). For any given pore surface charge, this electrification is a given function of the radius of the accessible part of the pore scaled by the Debye length without regard to the Bjerrum parameter or the bulk concentration of the electrolyte and without regard to the pore size relative to the ion diameter. If an additional uniform electric potential is applied in the pore, the electrification changes. At a certain potential the pore is electroneutral. This potential is an approximation to the Donnan potential in a "Swiss cheese" membrane model taking into account interactions of ions inside each pore, but replacing the detailed interactions between ions in different pores with a mere neutralizing collective potential. The deviations from electroneutrality, the mean ion occupation numbers and the average mean ion activity coefficients in the pores are investigated as a function of the total applied potential (the external potential + the potential from the surface charge). Also, the average single ion activity coefficients in the pores are investigated for different pore sizes and surface charges. Some consequences for the theory of ion exchange membranes are discussed. The results are also compared to a carricature analytical model for minimal pores containing no more than one ion at a time. The excess interaction energy between the ions in the pore, its variance and the average exponential of the configuration energy divided by kT is also sampled in each simulation. From the variance, the excess heat capacity at constant volume with a correction term for number fluctuations is calculated. From the logarithm of the average exponential of the interaction energy, the electrostatic Helmholtz free energy in the bulk limit may be extrapolated (very large pores). These excess quantities per particle are scaled by the reciprocal of the radius of the accessible sphere measured in Debye lengths. In neutral pores, the excess energy per particle is a fraction of the bulk value extrapolating monotonously to the bulk value for large pores.

KEY WORDS: Spherical charged pores, primitive model electrolytes, spontaneous electrification, Donnan potentials, activity coefficients in pores, excess energy, Grand Canonical Ensemble Monte Carlo

*To whom all correspondence should be sent.

INTRODUCTION

In a previous paper [1] one of us (TSS) has reported some results from Grand Canonical Ensemble Monte Carlo (GCEMC) simulations of restricted primitive model electrolytes in small, spherical, charged or non-charged pores. The dielectric permittivities of the pores and of the pore walls were taken as identical. The present study is a continuation of this work, but the number of simulations and of different situations are much larger, and the simulations are run with more configurations. The conclusions reached here will therefore rest on a firmer basis.

The sorption of electrolytes in charged micropores are important in many applications, for example in industrial ion exchange membranes, in reverse micelles and microemulsions, in natural clays and in zeolithes, in polymeric ion conductors, and in cavities in transmembrane proteins for ionic transport in the living cell. The electrification of small water droplets in thunderclouds is another important example of the interest of such systems. In all of these cases, the difference in dielectric permittivity between the two phases is of importance. To include such effects is not a simple matter, however, since there is no generalisation of the image charge concept to spherical geometry. We intend to return to more realistic systems with different dielectric permittivities in a later publication, but even in the case of equal dielectric permittivities reference [1] indicated that a lot of interesting effects appeared, which should be further scrutinized. Before these effects are clearly understood, we shall have no hope of understanding additional effects of different dielectric permittivities and/or different ionic diameters.

In the present paper, we discuss first the *basic input and output data* of the GCEMC computer programme and list tables of the simulations performed and the main results. In the next section, the *spontaneous electrification* of a pore in equilibrium with an external bulk solution is discussed. Then, the *regulation of the electrification* of the pores as a function of an *applied potential* is discussed. In macrosystems with a lot of spherical pores such as a "Swiss cheese" ion exchange membrane, deviations from electroneutrality of the pores are smaller and smaller as the size of the membrane phase increases [1]. We should mention in passing, that impedance measurements seem to indicate, that small spherical micropores exist in the skin layer of at least some reverse osmosis desalination membranes [2, 3, 4].

In an infinite membrane phase, all pores have to be electroneutral not to have an infinite electrostatic energy density. The pores may be forced to electroneutrality by a *collectively generated potential* applied to each pore. We determine from a number of simulations the applied potential leading to electroneutrality in a given pore. This potential is a computational generalisation of the classical *Donnan potential* [5, 6] taking into account the interactions between the ions in a single pore and the effects of space restrictions in this pore. A more involved calculation treating also the detailed interactions between ions in different pores in *e.g.* lattice pore systems of increasing size would in principle be better, but computationally very difficult.

In the electrochemical characterisation of ion exchange membranes, the Donnan potentials are of great importance, see [3, 4] and the references herein, and so is the case in a lot of other practical situations such as ion exchange in clay and the measurement of osmotic pressure of protein solutions. In the present study, the Donnan potential is computed for a great variety of pore sizes and electrolytes.

After the Donnan potentials, we discuss the average *ion occupation numbers* in

the pores and the *average activity coefficients* of ions under space restrictions and double layer forces, and finally we discuss some other thermodynamic quantities for example the *excess interaction energy* of the ions in different pores. In appendix A, we summarize the methodology and nomenclature used in this treatise for easy reference for the readers, and in appendix B we treat a carricature, analytically solvable model for minimal pores, which are pores being able to accommodate only one ion at a time. This model has a behaviour with certain similarities to the behaviour found by GCEMC in non-minimal pores, but is also strikingly different. Anyway, it is interesting as a limiting case of extremely small pores.

THE MODEL AND THE BASIC INPUT AND OUTPUT DATA

In GCEMC, the chemical potentials of the species are fixed to some values and the number of particles in the system are calculated as statistical averages. For ions, it is the *electrochemical potential* (*per* ion)

$$\mu_{i,el} = \mu_i(\text{ideal}) + \mu_i(\text{excess}) + z_i e_0 \Psi \tag{1}$$

which is fixed for each of the ionic species ($i = 1 \ldots n$). The electric potential is called Ψ, the valency of the ion z_i, and the elementary charge e_0. The *excess chemical potential* is the contribution from the ion-ion interactions. The system considered is an *open system* consisting of a spherical pore of radius R. The system is in some way in thermodynamical equilibrium with an *external electrolyte bath* with fixed electrolyte concentrations and with a fixed electric potential. The walls of the pore are considered *impenetrable* to the ions of diameter = a. The dimensionless parameter

$$\tau = (R/a) - 1/2 \tag{2}$$

is the radius of the part of the pore *accessible to the ions* scaled by the ionic diameter. There is a certain conceptual conflict in regarding the walls as impenetrable and still regarding the interior solution in the pore to be in matter equilibrium with an external medium. Then, at least sometimes, ions should be able to pass the wall. Nevertheless, in our GCEMC, we reject any configuration, where an ion has any overlap with the wall. Thus, one will never see an ion in the act of passing through the wall! One might resolve this paradox as a matter of time scales. The motion of the ions inside the pore is fast, and only *extremely seldomly* does some ion pass the wall. However, in thermodynamics we have plenty of time to wait, and therefore we have equilibrium with the external bath.

It is customary to fix the electric potential in the external *bulk solution* to $\Psi = 0$. Then, the input parameters are just the (single ion) chemical potentials of the ionic species present, and for a $z{:}z$ electrolyte with equal ionic diameters in a dielectric continuum (= the *Restricted Primitive Model*, RPM), the cation and anion *excess* chemical potentials are both equal to the mean ionic *excess* chemical potential (a measurable quantity). However, we may apply a certain electric potential to the pore phase. The difference between the electric potential in the pore and in the external bath we call $\Delta\Psi$. The *dimensionless applied potential* in the pore phase is defined as $\Delta = e_0\Delta\Psi/kT$. It shows up to be more expedient, however, to assume the electric potential in the pore phase (before the introduction of the pore surface charge)

to be zero. Then, the dimensionless electric potential in the *bulk solution* is $-\Delta$ and we have:

$$\mu_{\text{cation},el}/kT = \mu_{\text{cation}}(\text{bulk})/\kappa T - z_{\text{cation}}\Delta \tag{3a}$$

$$\mu_{\text{anion},el}/kT = \mu_{\text{anion}}(\text{bulk})/kT + z_{\text{anion}}\Delta \tag{3b}$$

For any given ion (i) we have

$$\mu_i(\text{bulk})/kT = \ln(\Lambda_i^3 Z_i) \tag{4}$$

where Λ_i is the thermal deBroglie wavelength of the ion, and Z_i is an *absolute single ion activity* of dimension volume^{-1}. The bulk chemical potential may be split into an *ideal* term and an *excess* term:

$$\mu_i(\text{bulk})/kT = \mu_i(\text{ideal})/kT + \mu_i(\text{excess})/kT = \ln(\Lambda_i^3\rho_i) + \ln(Z_i/\rho_i) \tag{5}$$

where ρ_i is the ion density. For the restricted primitive model (RPM) we have:

$$z_{\text{cation}} = -z_{\text{anion}} = z \tag{6}$$

$$\mu_{\text{cation}}(\text{excess}) = \mu_{\text{anion}}(\text{excess}) \tag{7}$$

In the case of the RPM we have:

$$\rho_{\text{cation}} = \rho_{\text{anion}} \tag{8}$$

$$Z_{\text{cation}} = Z_{\text{anion}} = Z_{\pm} \tag{9}$$

where is the *absolute mean ionic activity* of dimension volume^{-1}. Thus, as the basic input parameters characteristic for the *bulk solution* we shall take the *dimensionless absolute mean ionic activity*

$$Z_{\pm}^{*} = a^3 Z_{\pm} \tag{10}$$

together with the *dimensionless bulk electric potential* ($-\Delta$). The basic characteristics of the RPM *electrolyte* is the *Bjerrum parameter* (B) or the *reduced Bjerrum parameter* (B_r) and the *dimensionless total ion density* (ρ^*)

$$\mathrm{B} = z^2 e_0^2/(4\pi\varepsilon kT a) = z^2 \mathrm{B}_r \tag{11}$$

$$\rho^* = a^3(\rho_{\text{cation}} + \rho_{\text{anion}}) \tag{12}$$

from which quantities we may calculate

$$\kappa a = \sqrt{(4\pi \mathrm{B}\rho^*)} \tag{13}$$

where $1/\kappa$ is the *Debye length*. The Bjerrum parameter is also necessary for the evaluation of the electrostatic interactions between the ions in the pore (see the appendix). The input value of $Z_{\pm}^{*}$ can be evaluated from ρ^* and the *mean ionic activity coefficient* ($y_{\pm}$) in the bulk electrolyte, since we have (for the RPM):

$$\begin{aligned}\mu_{\pm}(\text{excess})/kT = \ln y_{\pm} &= (1/2)\ln\{(Z_+ Z_-)/(\rho_+\rho_-)\} \\ &= \ln(Z_+/\rho_+) = \ln(2Z_{\pm}^{*}/\rho^*)\end{aligned} \tag{14}$$

The value of $\mu_{\pm}(\text{excess})/kT$ or of the mean ionic activity coefficient may for a given electrolyte be found for example by Canonical Ensemble Monte Carlo calculations following the Widom approach [7, 8] with electrostatic corrections for the

introduction of the "test ion" as described in recent publications [3, 9, 10, 11].

It should be noticed, that we are not able to determine whether for example a high value of B is due to a high charge z (2:2 or even 3:3 electrolyte), or if the electrolyte is a 1:1 electrolyte with very small ionic diameters, or whether it is dissolved in a medium with low dielectric coefficient (as in polymer membranes). However, the valency z of the RPM electrolyte *is* involved in the calculation of the average net charge (or electrification) of a pore to be discussed shortly. And the valencies z and $-z$ of the cation and anion *are* involved in the GCEMC simulation, because of (1) their appearance in the input for $\Delta \neq 0$ - see Equations (3a-b) - and (2) their appearance in a dimensionless energy term of magnitude $\pm z\,(Q/e_0)\,(B/z^2)\,(a/R)$ for insertion of the ion into the basic electric potential in the pore (before the interactions with other ions) - see Equation (16) later on and the appendix. However, a given simulation with a given B and ρ^* (and a corresponding value of $Z_\pm$) is valid for any $z{:}z$ electrolyte, even if z has been put to unity. This is so since, if we have a 2:2 electrolyte, the same electrochemical potentials in the bulk will appear, when the external potential $-\Delta$ is halved. Similarly, the same values of the terms $\pm\,(Q/e_0)\,(B/z)\,(a/R)$ will be used in the GCEMC programme, if Q/e_0 is replaced by $2Q/(e_0)$. Therefore, we shall speak about z - *invariance* of the results of the simulation for a 1:1 RPM electrolyte, when we instead of the surface charge Q/e_0 have a surface charge $= zQ/e_0$ and instead of the external potential $-\Delta$ have a potential $-(\Delta/z)$.

Thus, for the RPM there are 6 basic *input parameters* for the GCEMC simulations: B, ρ^* (κa), $Z_\pm{}^*$, R/a, Δ and Q/e_0. The latter quantity is the *pore charge* Q measured in units of the elementary charge. To retain the spherical symmetry, the pore charge is thought to be smeared out uniformly on the inside surface of the spherical pore. The valency z need only to be considered to have the wanted input for in a z-invariant 1:1 simulation.

The detailed procedure of the simulation is described in the appendix. The *output parameters* from the simulations are the average population numbers of cations and anions ($\langle N_+ \rangle$ and $\langle N_- \rangle$) and the *variances* based on the *individual configurations* of these quantities. We have also expanded the programme to be able to calculate the *average excess mutual interaction energy* of the fluctuating number of ions in the pore and the variance of this quantity and also to calculate the average of the exponential of the dimensionless configurational energies. These quantities will be discussed later on.

Table 1 exhibits a survey over the simulations performed by listing the input parameters. The simulation numbers commence with no. 51. This is in order to be able to refer to the simulations in reference [1] as nos. 1-50, see Table 1 in this paper. Table 2 shows the results for the average population numbers and the fluctuation variances together with a listing of the number of configurations used in the different simulations. Finally, in Table 3, the results for the average electrostatic interaction energy (ion-ion, ion-wall charge) $\langle U/kT \rangle$ as well as $\langle \exp(U/kT) \rangle$ and their fluctuation variances are shown.

We have also sampled *distribution functions* in the pores for the cations and the anions as a function of the radial position in the pore like in reference [1]. The discussion of these results, however, will be postponed to a future publication, where we shall also study the influence of having different ionic radii.

Table 1 Survey of **GCEMC** simulations performed.

No	*B*	*κa*	$Z^*_{\pm}$	*Q/eo*	*R/a*	Δ
51	1.546	0.139383	4.5409e−4	0	5	0
52	1.546	0.139383	4.5409e−4	0	5	4
53	1.546	0.139383	4.5409e−4	0	5	8
54	1.546	0.139383	4.5409e−4	0	10	0
55	1.546	0.139383	4.5409e−4	0	10	4
56	1.546	0.139383	4.5409e−4	0	10	8
57	1.546	0.139383	4.5409e−4	0	15	0
58	1.546	0.139383	4.5409e−4	0	15	4
59	1.546	0.139383	4.5409e−4	0	15	8
60	1.546	0.139383	4.5409e−4	0	25	0
61	1.546	0.139383	4.5409e−4	0	35	0
62	1.546	0.139383	4.5409e−4	1	5	−0.3092
63	1.546	0.139383	4.5409e−4	1	5	−0.3
64	1.546	0.139383	4.5409e−4	1	5	−0.2
65	1.546	0.139383	4.5409e−4	1	5	−0.1
66	1.546	0.139383	4.5409e−4	1	5	0
67	1.546	0.139383	4.5409e−4	1	5	1.8063
68	1.546	0.139383	4.5409e−4	1	5	2
69	1.546	0.139383	4.5409e−4	1	5	4
70	1.546	0.139383	4.5409e−4	1	5	6
71	1.546	0.139383	4.5409e−4	1	5	8
72	1.546	0.139383	4.5409e−4	1	10	−0.1546
73	1.546	0.139383	4.5409e−4	1	10	−0.15
74	1.546	0.139383	4.5409e−4	1	10	−0.10
75	1.546	0.139383	4.5409e−4	1	10	−0.05
76	1.546	0.139383	4.5409e−4	1	10	0
77	1.546	0.139383	4.5409e−4	1	10	0.3245
78	1.546	0.139383	4.5409e−4	1	10	2
79	1.546	0.139383	4.5409e−4	1	10	4
80	1.546	0.139383	4.5409e−4	1	10	6
81	1.546	0.139383	4.5409e−4	1	10	8
82	1.546	0.139383	4.5409e−4	1	15	−1.0306
83	1.546	0.139383	4.5409e−4	1	15	−0.09
84	1.546	0.139383	4.5409e−4	1	15	−0.06
85	1.546	0.139383	4.5409e−4	1	15	−0.03
86	1.546	0.139383	4.5409e−4	1	15	0
87	1.546	0.139383	4.5409e−4	1	15	0.1035
88	1.546	0.139383	4.5409e−4	1	15	2
89	1.546	0.139383	4.5409e−4	1	15	4
90	1.546	0.139383	4.5409e−4	1	15	6
91	1.546	0.139383	4.5409e−4	1	15	8
92	1.546	0.139383	4.5409e−4	5	5	−1.546
93	1.546	0.139383	4.5409e−4	5	5	−1.5
94	1.546	0.139383	4.5409e−4	5	5	−1.0
95	1.546	0.139383	4.5409e−4	5	5	−0.5
96	1.546	0.139383	4.5409e−4	5	5	0
97	1.546	0.139383	4.5409e−4	5	5	2
98	1.546	0.139383	4.5409e−4	5	5	3
99	1.546	0.139383	4.5409e−4	5	5	3.3
100	1.546	0.139383	4.5409e−4	5	5	3.5
101	1.546	0.139383	4.5409e−4	5	5	3.596
102	1.546	0.139383	4.5409e−4	5	5	3.6
103	1.546	0.139383	4.5409e−4	5	5	3.7
104	1.546	0.139383	4.5409e−4	5	5	3.8
105	1.546	0.139383	4.5409e−4	5	5	4.0
106	1.546	0.139383	4.5409e−4	5	5	6.0

Table 1 *continued*

No	*B*	*κa*	$Z^*_{\pm}$	*Q/eo*	*R/a*	Δ
107	1.546	0.139383	4.5409e−4	5	5	8.0
108	1.546	0.139383	4.5409e−4	5	10	−0.773
109	1.546	0.139383	4.5409e−4	5	10	−0.6
110	1.546	0.139383	4.5409e−4	5	10	−0.4
111	1.546	0.139383	4.5409e−4	5	10	−0.2
112	1.546	0.139383	4.5409e−4	5	10	0
113	1.546	0.139383	4.5409e−4	5	10	1.3280
114	1.546	0.139383	4.5409e−4	5	10	2
115	1.546	0.139383	4.5409e−4	5	10	4
116	1.546	0.139383	4.5409e−4	5	10	6
117	1.546	0.139383	4.5409e−4	5	10	8
118	1.546	0.139383	4.5409e−4	5	15	−0.5153
119	1.546	0.139383	4.5409e−4	5	15	−0.4
120	1.546	0.139383	4.5409e−4	5	15	−0.3
121	1.546	0.139383	4.5409e−4	5	15	−0.1
122	1.546	0.139383	4.5409e−4	5	15	0
123	1.546	0.139383	4.5409e−4	5	15	0.5032
124	1.546	0.139383	4.5409e−4	5	15	2
125	1.546	0.139383	4.5409e−4	5	15	4
126	1.546	0.139383	4.5409e−4	5	15	6
127	1.546	0.139383	4.5409e−4	5	15	8
128	1.546	0.139383	4.5409e−4	5	25	0
129	1.546	0.139383	4.5409e−4	5	35	0
130	1.546	0.139383	4.5409e−4	10	5	−3.092
131	1.546	0.139383	4.5409e−4	10	5	−3
132	1.546	0.139383	4.5409e−4	10	5	−2
133	1.546	0.139383	4.5409e−4	10	5	−1
134	1.546	0.139383	4.5409e−4	10	5	0
135	1.546	0.139383	4.5409e−4	10	5	2
136	1.546	0.139383	4.5409e−4	10	5	4
137	1.546	0.139383	4.5409e−4	10	5	4.5722
138	1.546	0.139383	4.5409e−4	10	5	6
139	1.546	0.139383	4.5409e−4	10	5	8
140	1.546	0.139383	4.5409e−4	10	10	−1.546
141	1.546	0.139383	4.5409e−4	10	10	−1.5
142	1.546	0.139383	4.5409e−4	10	10	−1.0
143	1.546	0.139383	4.5409e−4	10	10	−0.5
144	1.546	0.139383	4.5409e−4	10	10	0
145	1.546	0.139383	4.5409e−4	10	10	2
146	1.546	0.139383	4.5409e−4	10	10	2.0780
147	1.546	0.139383	4.5409e−4	10	10	4
148	1.546	0.139383	4.5409e−4	10	10	6
149	1.546	0.139383	4.5409e−4	10	10	8
150	1.546	0.139383	4.5409e−4	10	15	−1.0306
151	1.546	0.139383	4.5409e−4	10	15	−0.9
152	1.546	0.139383	4.5409e−4	10	15	−0.6
153	1.546	0.139383	4.5409e−4	10	15	−0.3
154	1.546	0.139383	4.5409e−4	10	15	0
155	1.546	0.139383	4.5409e−4	10	15	0.9480
156	1.546	0.139383	4.5409e−4	10	15	2
157	1.546	0.139383	4.5409e−4	10	15	4
158	1.546	0.139383	4.5409e−4	10	15	6
159	1.546	0.139383	4.5409e−4	10	15	8
160	1.681	0.911141	1.5166e−2	0	1	0
161	1.681	0.911141	1.5166e−2	0	2	0
162	1.681	0.911141	1.5166e−2	0	3	0

Table 1 *continued*

No	*B*	*κa*	$Z^*_\pm$	*Q/eo*	*R/a*	Δ
163	1.681	0.911141	1.5166e−2	0	4	0
164	1.681	0.911141	1.5166e−2	0	5	0
165	1.681	0.911141	1.5166e−2	5	2	0
166	1.681	0.911141	1.5166e−2	5	3	0
167	1.681	0.911141	1.5166e−2	5	4	0
168	1.681	0.911141	1.5166e−2	5	5	0
169	1.681	0.911141	1.5166e−2	10	2	0
170	1.681	0.911141	1.5166e−2	10	3	0
171	1.681	0.911141	1.5166e−2	10	4	0
172	1.681	0.911141	1.5166e−2	10	5	0
173	1.681	1.39769	4.0847e−2	0	1	0
174	1.681	1.39769	4.0847e−2	0	1.5	0
175	1.681	1.39769	4.0847e−2	0	2	0
176	1.681	1.39769	4.0847e−2	0	2.5	0
177	1.681	1.39769	4.0847e−2	0	3	0
178	1.681	1.39769	4.0847e−2	0	3.5	0
179	1.681	1.39769	4.0847e−2	5	1.5	0
180	1.681	1.39769	4.0847e−2	5	2	0
181	1.681	1.39769	4.0847e−2	5	2.5	0
182	1.681	1.39769	4.0847e−2	5	3	0
183	1.681	1.39769	4.0847e−2	5	3.5	0
184	1.681	1.39769	4.0847e−2	10	1.5	0
185	1.681	1.39769	4.0847e−2	10	2	0
186	1.681	1.39769	4.0847e−2	10	2.5	0
187	1.681	1.39769	4.0847e−2	10	3	0
188	1.681	1.39769	4.0847e−2	10	3.5	0
189	2.0	2.2420e−2	9.7820e−6	0	5	0
190	2.0	2.2420e−2	9.7820e−6	0	10	0
191	2.0	2.2420e−2	9.7820e−6	0	15	0
192	2.0	2.2420e−2	9.7820e−6	0	25	0
193	2.0	2.2420e−2	9.7820e−6	0	35	0
194	2.0	2.2420e−2	9.7820e−6	1	5	5.6027
195	2.0	2.2420e−2	9.7820e−6	1	10	3.3661
196	2.0	2.2420e−2	9.7820e−6	1	15	2.1125
197	2.0	2.2420e−2	9.7820e−6	5	5	0
198	2.0	2.2420e−2	9.7820e−6	5	5	7.4432
199	2.0	2.2420e−2	9.7820e−6	5	10	0
200	2.0	2.2420e−2	9.7820e−6	5	10	5.0830
201	2.0	2.2420e−2	9.7820e−6	5	15	0
202	2.0	2.2420e−2	9.7820e−6	5	15	3.7812
203	2.0	2.2420e−2	9.7820e−6	5	25	0
204	2.0	2.2420e−2	9.7820e−6	5	35	0
205	2.0	2.2420e−2	9.7820e−6	10	5	0
206	2.0	2.2420e−2	9.7820e−6	10	5	8.4620
207	2.0	2.2420e−2	9.7820e−6	10	10	0
208	2.0	2.2420e−2	9.7820e−6	10	10	5.9223
209	2.0	2.2420e−2	9.7820e−6	10	15	0
210	2.0	2.2420e−2	9.7820e−6	10	15	4.5731
211	2.0	2.2420e−2	9.7820e−6	10	25	0
212	2.0	2.2420e−2	9.7820e−6	10	35	0
213	2.0	1.1210e−1	2.2594e−4	0	5	0
214	2.0	1.1210e−1	2.2594e−4	0	10	0
215	2.0	1.1210e−1	2.2594e−4	0	15	0
216	2.0	1.1210e−1	2.2594e−4	0	25	0
217	2.0	1.1210e−1	2.2594e−4	0	35	0
218	2.0	1.1210e−1	2.2594e−4	1	5	2.4694

Table 1 *continued*

No	*B*	*κa*	$Z^*_{\pm}$	*Q/eo*	*R/a*	Δ
219	2.0	1.1210e−1	2.2594e−4	1	10	6.0271
220	2.0	1.1210e−1	2.2594e−4	1	15	1.9311
221	2.0	1.1210e−1	2.2594e−4	5	5	0
222	2.0	1.1210e−1	2.2594e−4	5	5	4.3039
223	2.0	1.1210e−1	2.2594e−4	5	10	0
224	2.0	1.1210e−1	2.2594e−4	5	10	1.9732
225	2.0	1.1210e−1	2.2594e−4	5	15	0
226	2.0	1.1210e−1	2.2594e−4	5	15	0.87831
227	2.0	1.1210e−1	2.2594e−4	5	25	0
228	2.0	1.1210e−1	2.2594e−4	5	35	0
229	2.0	1.1210e−1	2.2594e−4	10	5	0
230	2.0	1.1210e−1	2.2594e−4	10	5	5.3210
231	2.0	1.1210e−1	2.2594e−4	10	10	0
232	2.0	1.1210e−1	2.2594e−4	10	10	2.7902
233	2.0	1.1210e−1	2.2594e−4	10	15	0
234	2.0	1.1210e−1	2.2594e−4	10	15	1.5110
235	2.0	1.1210e−1	2.2594e−4	10	25	0
236	2.0	1.1210e−1	2.2594e−4	10	35	0
237	6.8116	2.7638e−2	4.0202e−6	0	5	0
238	6.8116	2.7638e−2	4.0202e−6	0	10	0
239	6.8116	2.7638e−2	4.0202e−6	0	15	0
240	6.8116	2.7638e−2	4.0202e−6	0	25	0
241	6.8116	2.7638e−2	4.0202e−6	0	35	0
242	6.8116	2.7638e−2	4.0202e−6	1	5	6.1696
243	6.8116	2.7638e−2	4.0202e−6	1	10	4.1615
244	6.8116	2.7638e−2	4.0202e−6	1	15	2.9468
245	6.8116	2.7638e−2	4.0202e−6	5	5	0
246	6.8116	2.7638e−2	4.0202e−6	5	5	8.0257
247	6.8116	2.7638e−2	4.0202e−6	5	10	0
248	6.8116	2.7638e−2	4.0202e−6	5	10	5.8954
249	6.8116	2.7638e−2	4.0202e−6	5	15	0
250	6.8116	2.7638e−2	4.0202e−6	5	15	4.6615
251	6.8116	2.7638e−2	4.0202e−6	5	25	0
252	6.8116	2.7638e−2	4.0202e−6	5	35	0
253	6.8116	2.7638e−2	4.0202e−6	10	5	0
254	6.8116	2.7638e−2	4.0202e−6	10	5	9.1320
255	6.8116	2.7638e−2	4.0202e−6	10	10	0
256	6.8116	2.7638e−2	4.0202e−6	10	10	6.7997
257	6.8116	2.7638e−2	4.0202e−6	10	15	0
258	6.8116	2.7638e−2	4.0202e−6	10	15	5.5318
259	6.8116	2.7638e−2	4.0202e−6	10	25	0
260	6.8116	2.7638e−2	4.0202e−6	10	35	0

$Z^*_{\pm}$ evaluated by equation 14. The values of $\mu_{\pm}$(excess)/kT for B = 1.546, 2 and 6.8116 have been taken from extrapolated CEMC simulations, reference 10. The values of $\mu_{\pm}$(excess)/kT for B = 1.681 have been taken from the HNC calculations in reference 9.

Table 2 Occupation numbers, their respective variances and the total number of configurations.

No.	$\langle N+\rangle$	$\langle N-\rangle$	$VAR(N+)$	$VAR(N-)$	*config.* $\times 10^{-6}$
51	1.7810e−1	1.7820e−1	1.6910e−1	1.6927e−1	60
52	1.2680e−2	3.1590e+0	1.2662e−2	1.4749e+0	15
53	4.7391e−3	1.0733e+1	4.7412e−3	2.1859e+0	15
54	1.7275e+0	1.7279e+0	1.4182e+0	1.4187e+0	60
55	3.0018e−1	1.1701e+1	2.9586e−1	3.9446e+0	15
56	1.5091e−1	2.9067e+1	1.5004e−1	4.9272e+0	15
57	6.2228e+0	6.2225e+0	4.4525e+0	2.1101e+0	60
58	9.0817e−1	2.3750e+1	1.7397e+0	7.3140e+0	15
59	1.0481e+0	5.0847e+1	1.0279e+0	8.2789e+0	15
60	3.0319e+1	3.0315e+1	1.8584e+1	1.8605e+1	60
61	8.4934e+1	8.4932e+1	4.8228e+1	4.8130e+1	60
62	1.7830e−1	1.7841e−1	1.6917e−1	1.6944e−1	20
63	1.7692e−1	1.7968e−1	1.6811e−1	1.7052e−1	20
64	1.6240e−1	1.9600e−1	1.5497e−1	1.8493e−1	20
65	1.4857e−1	2.1390e−1	1.4244e−1	2.0107e−1	20
66	1.3655e−1	2.3391e−1	1.1346e−1	2.1836e−1	60
67	3.3635e−2	1.0337e+0	3.3404e−2	7.6551e−1	60
68	2.9607e−2	1.1873e+0	2.9429e−2	8.4378e−1	60
69	1.1193e−2	3.6258e+0	1.1170e−2	1.5646e+0	60
70	6.3675e−3	7.2014e+0	6.3587e−3	1.9831e+0	60
71	4.3898e−3	1.1410e+1	4.3888e−3	2.2124e+0	60
72	1.7277e+0	1.7269e+0	1.1903e+0	1.4174e+0	20
73	1.7231e+0	1.7329e+0	1.4126e+0	1.4206e+0	20
74	1.6726e+0	1.7842e+0	1.3805e+0	1.4518e+0	20
75	1.3016e+0	2.3030e+0	1.1315e+0	1.7496e+0	60
76	1.5745e+0	1.8944e+0	1.3174e+0	1.5178e+0	60
77	1.3006e+0	2.3016e+0	1.1311e+0	1.7472e+0	15
78	5.5707e−1	5.7104e+0	5.3332e−1	2.9798e+0	60
79	2.8879e−1	1.2288e+1	2.8461e−1	4.0004e+0	60
80	1.9270e−1	2.0553e+1	1.9137e−1	4.5786e+0	60
81	1.4837e−1	2.9801e+1	1.4777e−1	4.9323e+0	60
82	6.2259e+0	6.2260e+0	4.4434e+0	4.4556e+0	20
83	6.1934e+0	6.2589e+0	4.4394e+0	4.4754e+0	20
84	6.1184e+0	6.3301e+0	4.4113e+0	4.5030e+0	20
85	6.0460e+0	6.3995e+0	4.3764e+0	4.5236e+0	20
86	5.9804e+0	6.4815e+0	4.3491e+0	4.5574e+0	60
87	5.7444e+0	6.7453e+0	4.2454e+0	4.6632e+0	75
88	2.9562e+0	1.3638e+1	2.6350e+0	6.3147e+0	60
89	1.7992e+0	2.4361e+1	1.7106e+0	7.3603e+0	60
90	1.2949e+0	3.7312e+1	1.2583e+0	7.9489e+0	60
91	1.0359e+0	5.1609e+1	1.0146e+0	8.3184e+0	60
92	1.7852e−1	1.7850e−1	1.6963e−1	1.6955e−1	20
93	1.7115e−1	1.8557e−1	1.6301e−1	1.7589e−1	20
94	1.1136e−1	2.8733e−1	1.0799e−1	2.6378e−1	20
95	7.3566e−2	4.4196e−1	7.2164e−2	3.8716e−1	20
96	4.9943e−2	6.6819e−1	4.9367e−2	5.4767e−1	60
97	1.5306e−2	2.5245e+0	1.5271e−2	1.3259e+0	60
98	1.0385e−2	4.0018e+0	1.0373e−2	1.6272e+0	60
99	9.4295e−3	4.4990e+0	9.4141e−3	1.7026e+0	60
100	8.8306e−3	4.8444e+0	8.8258e−3	1.7489e+0	60
101	8.5749e−3	5.0117e+0	8.5679e−3	1.7699e+0	60
102	8.5272e−3	5.0187e+0	8.5293e−3	1.7710e+0	60
103	8.3413e−3	5.1951e+0	8.3242e−3	1.7914e+0	60
104	8.1085e−3	5.3738e+0	8.1035e−3	1.8119e+0	60
105	7.6133e−3	5.7415e+0	7.6052e−3	1.8504e+0	60
106	4.9556e−3	9.7519e+0	4.9575e−3	2.1430e+0	60

Table 2 *continued*

No.	$\langle N+\rangle$	$\langle N-\rangle$	$VAR(N+)$	$VAR(N-)$	*config.* $\times 10^{-6}$
107	3.7117e−3	1.4209e+1	3.7111e−3	2.3095e+0	60
108	1.7266e+0	1.7261e+0	1.4166e+0	1.4143e+0	20
109	1.5574e+0	1.9179e+0	1.3051e+0	1.5336e+0	20
110	1.3857e+0	2.1601e+0	1.1896e+0	1.6699e+0	20
111	1.2327e+0	2.4340e+0	1.0823e+0	1.8179e+0	20
112	1.1003e+0	2.7393e+0	9.8249e−1	1.9669e+0	60
113	5.6959e−1	5.5671e+0	5.4506e−1	2.9402e+0	60
114	4.3783e−1	7.4974e+0	4.2547e−1	3.3586e+0	60
115	2.4921e−1	1.4700e+1	2.4625e−1	4.2197e+0	60
116	1.7565e−1	2.3328e+1	1.7448e−1	4.7033e+0	60
117	1.3950e−1	3.2798e+1	1.3894e−1	5.0161e+0	60
118	6.2162e+0	6.2225e+0	4.4451e+0	4.4493e+0	20
119	5.9560e+0	6.5149e+0	4.3412e+0	4.5619e+0	20
120	5.7240e+0	6.7655e+0	4.2357e+0	4.6684e+0	20
121	5.3072e+0	7.3259e+0	4.0401e+0	4.8720e+0	20
122	5.1054e+0	7.6114e+0	3.9446e+0	4.9758e+0	60
123	4.2372e+0	9.2369e+0	3.4695e+0	5.4408e+0	60
124	2.6225e+0	1.5601e+1	2.3854e+0	6.5945e+0	60
125	1.6625e+0	1.6887e+1	1.5918e+0	7.5371e+0	60
126	1.2289e+0	4.0170e+1	1.1956e+0	8.0354e+0	60
127	9.9927e−1	5.4671e+1	9.7982e−1	8.3685e+0	60
128	2.8649e+1	3.2103e+1	1.8123e+1	1.8812e+1	30
129	8.3044e+1	8.6924e+1	4.8084e+1	4.8737e+1	30
130	1.7825e−1	1.7830e−1	1.6933e−1	1.6924e−1	20
131	1.6490e−1	1.9318e−1	1.5704e−1	1.8251e−1	20
132	7.0890e−2	4.5926e−1	6.9581e−2	3.9989e−1	20
133	3.4058e−2	1.0140e+0	3.3857e−2	7.5346e−1	20
134	1.9102e−2	1.9639e+0	1.9032e−2	1.1576e+0	60
135	8.6644e−3	4.9240e+0	8.6530e−3	1.7575e+0	60
136	5.4056e−3	8.7936e+0	5.4046e−3	2.0874e+0	60
137	4.9149e−3	1.0007e+1	4.9070e−3	2.1532e+0	60
138	3.9401e−3	1.3167e+1	3.9404e−3	2.2789e+0	60
139	3.1650e−3	1.7853e+1	3.1675e−3	2.4006e+0	60
140	1.7273e+0	1.7291e+0	1.4157e+0	1.4185e+0	20
141	1.6825e+0	1.7252e+0	1.3867e+0	1.4451e+0	20
142	1.2533e+0	2.3965e+0	1.0972e+0	1.7975e+0	20
143	9.4662e−1	3.2027e+0	8.6244e−1	2.1751e+0	20
144	7.3370e−1	4.2171e+0	6.8858e−1	2.5548e+0	60
145	3.4053e−1	1.0058e+1	3.3416e−1	3.7503e+0	60
146	3.3312e−1	1.0335e+1	3.2732e−1	3.7829e+0	60
147	2.1393e−1	1.7907e+1	2.1204e−1	4.4375e+0	60
148	1.5885e−1	2.6908e+1	1.5792e−1	4.8378e+0	60
149	1.3003e+1	3.6616e+1	1.2946e−1	5.1026e+0	60
150	6.2276e+0	6.2248e+0	4.4584e+0	4.4479e+0	20
151	5.9134e+0	6.5474e+0	4.3237e+0	4.5746e+0	20
152	5.2701e+0	7.3639e+0	4.0195e+0	4.8822e+0	20
153	4.7030e+0	8.2674e+0	3.7322e+0	5.1755e+0	20
154	4.2204e+0	9.2802e+0	3.4603e+0	5.4603e+0	60
155	3.0678e+0	1.3070e+1	2.7155e+0	6.2237e+0	60
156	2.2876e+0	1.8251e+1	2.1207e+0	6.8917e+0	60
157	1.5188e+0	3.0154e+1	1.4617e+0	7.6704e+0	60
158	1.1562e+0	4.3806e+1	1.1297e+0	8.1261e+0	60
159	9.5799e−1	5.8554e+1	9.4278e−1	8.4425e+0	60
160	7.7308e−3	7.7698e−3	7.6710e−3	7.7094e−3	30
161	2.3281e−1	2.3286e−1	2.0032e−1	2.0043e−1	30
162	1.1804e+0	1.1812e+0	8.2200e−1	8.2364e−1	30

Table 2 *continued*

No.	$\langle N+\rangle$	$\langle N-\rangle$	$VAR(N+)$	$VAR(N-)$	*config.* $\times 10^{-6}$
163	3.3498e+0	3.3495e+0	2.0376e+0	2.0405e+0	30
164	7.2164e+0	7.2161e+0	4.0820e+0	4.0824e+0	30
165	2.1582e−2	1.9996e+0	2.1294e−2	6.1387e−1	30
166	4.6225e−1	3.0922e+0	4.1010e−1	1.1672e+0	30
167	2.1575e+0	5.3057e+0	1.6140e+0	2.3115e+0	30
168	5.7260e+0	9.2305e+0	3.7423e+0	4.3358e+0	30
169	3.4430e−3	4.7967e+0	3.4369e−3	7.0529e−1	30
170	2.3496e−1	5.9362e+0	2.2135e−1	1.2851e+0	30
171	1.5048e+0	7.9600e+0	1.2440e+0	2.4082e+0	30
172	4.6557e+0	1.1724e+1	3.3327e+0	1.4189e+0	30
173	2.0603e−2	2.0383e−2	2.0179e−2	1.9968e−2	30
174	1.6901e−1	1.6912e−1	1.4561e−1	1.4569e−1	30
175	6.2267e−1	6.2265e−1	4.2871e−1	4.2867e−1	30
176	1.5206e+0	1.5200e+0	8.8044e−1	8.8120e−1	30
177	3.0060e+0	3.0045e+0	1.5681e+0	1.5657e+0	30
178	5.2184e+0	5.2187e+0	2.5408e+0	2.5411e+0	30
179	2.5784e−3	2.0232e+0	2.5720e−3	4.1727e−1	30
180	9.4412e−2	2.6607e+0	8.9317e−2	6.7234e−1	30
181	5.9062e−1	3.5677e+0	4.7752e−1	1.0790e+0	30
182	1.7629e+0	5.0504e+0	1.1195e+0	1.7448e+0	30
183	3.7551e+0	7.2785e+0	2.2087e+0	2.6926e+0	30
184	1.9666e−5	4.3741e+0	1.9666e−5	4.0802e−1	30
185	1.6432e−2	5.5047e+0	1.6251e−2	7.1689e−1	30
186	2.5739e−1	6.4284e+0	2.3198e−1	1.0921e+0	30
187	1.1023e+0	7.7934e+0	8.4660e−1	1.7447e+0	30
188	2.7876e+0	9.8913e+0	1.8411e+0	2.7075e+0	30
189	3.8404e−3	3.8252e−3	3.8346e−3	3.8201e−3	60
190	3.5927e−2	3.5942e−2	3.5671e−2	3.5665e−2	60
191	1.2763e−1	1.2815e−1	1.2527e−1	1.2591e−1	60
192	6.0754e−1	6.0745e−1	5.7752e−1	5.7751e−1	60
193	1.6994e+0	1.7000e+0	1.5452e+0	1.5460e+0	60
194	1.6533e−5	1.0002e+0	1.6533e−5	6.9860e−1	60
195	1.3265e−3	1.0006e+0	1.3259e−3	8.1916e−1	60
196	1.5921e−2	1.0172e+0	1.5888e−2	8.8307e−2	60
197	5.2503e−4	2.7751e−2	5.2495e−4	2.7446e−2	30
198	5.1833e−6	5.0010e+0	5.1833e−6	1.5013e+0	60
199	1.3500e−2	9.0666e−2	1.3463e−2	9.4261e−2	30
200	3.0488e−4	5.0000e+0	3.0479e−4	2.3267e+0	60
201	6.7909e−2	2.4233e−1	6.7280e−2	2.3369e−1	30
202	3.5640e−3	5.0020e+0	3.5604e−3	2.8324e+0	60
203	4.2548e−1	8.6807e−1	4.1075e−1	8.0644e−1	30
204	1.3511e+0	2.1423e+0	1.2538e+0	1.8986e+0	30
205	7.7166e−5	1.9349e−1	7.7160e−5	1.7978e−1	30
206	3.8000e−6	9.9993e+0	3.7999e−6	1.7757e+0	60
207	5.2359e−3	2.5150e−1	5.2340e−3	2.3860e−1	30
208	1.8530e−4	9.9987e+0	1.8526e−4	3.0433e+0	60
209	3.6222e−2	4.5393e−1	3.6048e−2	4.2500e−1	30
210	1.9434e−3	1.0001e+1	1.9434e−3	3.9570e+0	60
211	2.9893e−1	1.2346e+0	2.9172e−1	1.1119e+0	30
212	1.0756e+0	2.6960e+0	1.0155e+0	2.3124e+0	30
213	8.8766e−2	8.8537e−2	8.5985e−2	8.5759e−2	60
214	8.5805e−1	8.5889e−1	7.4703e−1	7.4839e−1	60
215	3.1040e+0	3.1028e+0	2.3956e+0	2.3944e+0	60
216	1.5159e+1	1.5158e+1	9.8639e+0	9.8578e+0	60
217	4.2558e+1	4.2558e+1	2.5445e+1	2.5420e+1	60
218	9.3367e−3	1.0086e+0	9.3226e−3	7.0383e−1	60

Table 2 *continued*

No.	$\langle N+ \rangle$	$\langle N- \rangle$	$VAR(N+)$	$VAR(N-)$	*config.* $\times 10^{-6}$
219	4.9907e−1	1.4982e+0	4.6457e−1	1.1610e+0	60
220	2.6420e+0	3.6453e+0	2.1381e+0	2.6612e+0	60
221	1.6482e−2	5.2186e−1	1.6404e−2	4.2972e−1	30
222	2.6646e−3	5.0030e+0	2.6626e−3	1.5025e+0	60
223	4.4006e−1	1.7112e+0	4.1436e−1	1.2786e+0	30
224	1.6482e−1	5.1707e+0	1.6249e−1	2.4240e+0	60
225	2.2458e+0	4.3140e+0	1.8928e+0	2.9454e+0	30
226	1.5260e+0	6.5184e+0	1.3857e+0	3.6674e+0	60
227	1.3682e+1	1.6796e+1	9.4221e+0	1.0291e+1	30
228	4.0753e+1	4.4388e+1	5.0097e+0	2.5782e+1	30
229	5.3363e−3	2.0020e+0	5.3352e−3	1.0519e+0	30
230	1.6432e−3	1.0001e+1	1.6427e−3	1.7763e+0	60
231	2.5127e−1	3.1657e+0	2.4443e−1	1.8941e+0	30
232	9.6299e−2	1.0095e+1	9.5678e−2	3.1060e+0	60
233	1.6643e+0	5.9227e+0	1.4873e+0	3.5006e+0	30
234	9.6292e−1	1.0961e+1	9.1898e−1	4.5253e+0	60
235	1.2393e+1	1.8634e+1	8.9637e+0	1.0727e+1	30
236	3.9101e+1	4.6386e+1	2.4821e+1	2.6139e+1	30
237	1.5537e−3	1.5536e−3	1.5513e−3	1.5524e−3	60
238	1.4812e−2	1.4759e−2	1.4708e−2	1.4646e−2	60
239	5.3300e−2	5.3279e−2	5.2256e−2	5.2255e−2	60
240	2.6079e−1	2.6079e−1	2.4561e−1	2.4563e−1	60
241	7.3659e−1	7.3649e−1	6.5797e−1	6.5716e−1	60
242	2.5750e−5	1.0007e+0	2.5749e−5	4.3353e−1	60
243	5.7601e−4	1.0024e+0	5.7605e−4	6.0398e−1	60
244	4.3610e−3	1.0031e+0	4.3568e−3	6.9040e−1	60
245	2.9866e−5	7.0475e−1	2.9865e−5	3.8571e−1	30
246	2.8100e−5	4.9980e+0	2.8099e−5	6.0704e−1	60
247	9.5326e−4	3.5685e−1	9.5289e−4	2.9518e−1	30
248	3.6768e−4	5.0007e+0	3.6754e−4	1.0797e+0	60
249	8.1507e−3	4.2090e−1	8.1240e−3	3.5702e−1	30
250	1.9781e−3	5.0012e+0	1.9771e−3	1.4504e+0	60
251	8.9831e−2	8.0567e−1	8.8391e−2	6.6190e−1	30
252	3.7458e−1	1.4934e+0	3.5721e−1	1.1676e+0	30
253	1.9400e−5	4.2690e+0	1.9399e−5	5.9491e−1	15
254	3.0683e−5	1.0000e+1	3.0682e−5	6.4766e−1	60
255	4.2460e−4	2.5112e+0	4.2441e−4	8.9737e−1	30
256	3.3378e−4	1.0002e+1	3.3393e−4	1.2183e+0	60
257	2.9073e−3	1.9834e+0	2.9046e−3	1.0223e+0	30
258	1.6426e−3	1.0014e+1	1.6417e−3	1.7102e+0	60
259	4.0943e−2	2.1115e+0	4.0737e−2	1.3148e+0	30
260	2.1382e−1	2.8340e+0	2.0955e−1	1.8122e+0	30

The variances of the mean occupation numbers are found by division of the tabulated variances by the number of configurations.

Table 3 Mean values of the configurational energy and of its exponential with their respective variances.

No.	$\langle U/kT \rangle$	$VAR(U/kT)$	$\langle exp(U/kT) \rangle$	$VAR(exp(U/kT))$
51	−1.2015e−2	1.3773e−2	9.9412e−1	1.2340e−2
54	−2.1647e−1	2.0927e−1	8.9340e−1	3.2219e−1
57	−9.4479e−1	8.0218e−1	5.9315e−1	2.9714e+0
60	−5.1930e+0	3.9536e+0	4.6604e−2	1.2068e+1
61	−1.5120e+1	1.1155e+1	1.5211e−3	1.3721e−1
67	−1.8547e−1	5.1989e−2		
77	−2.8915e−1	2.1718e−1		
87	−9.9045e−1	8.0555e−1		
101	−3.8671e+0	5.0222e−1		
113	−2.0105e+0	3.9667e−1		
123	−2.0847e+0	9.0422e−1		
137	−1.4755e+1	1.6543e+0		
146	−7.3102e+0	9.3429e−1		
155	−5.5113e+0	1.2188e+0		
189	−1.1871e−5	1.5259e−5	9.9999e−1	1.4691e−6
190	−2.3615e−4	2.7616e−4	9.9988e−1	2.2280e−4
191	−1.3117e−3	1.4451e−3	9.9935e−1	1.2997e−3
192	−9.9998e−3	1.0282e−2	9.9502e−1	1.0615e−2
193	−3.6866e−2	3.5573e−2	9.8137e−1	4.2385e−2
194	−2.4117e−1	5.9205e−2		
195	−1.0600e−1	2.1678e−2		
196	−6.7159e−2	1.2766e−2		
198	−5.1612e+0	6.5041e−1		
200	−2.4544e+0	3.1336e−1		
202	−1.5815e+0	1.9344e−1		
206	−1.9608e+1	2.1532e+0		
208	−9.5121e+0	1.0341e+0		
210	−6.1904e+0	6.4881e−1		
213	−5.4195e−3	7.0574e−3	9.9747e−1	5.2738e−3
214	−1.0336e−1	1.1372e−1	9.4979e−1	1.3152e−1
215	−4.7449e−1	4.6113e−1	7.7912e−1	1.0075e+0
216	−2.7100e+0	2.3084e+0	2.1607e−1	8.4863e+0
217	−8.0231e+0	6.5172e+0	1.0835e−2	3.7242e+1
218	−2.4500e−1	6.4834e−2		
219	−2.0375e−1	1.2803e−1		
220	−5.3418e−1	4.6373e−1		
222	−5.1645e+0	6.5550e−1		
224	−2.5284e+0	3.9682e−1		
226	−2.0004e+0	6.0080e−1		
230	−1.9615e+1	2.1524e+0		
232	−9.5763e+0	1.1142e+0		
234	−6.5598e+0	1.0316e+0		
237	−1.1611e−4	5.7587e−4	9.9997e−1	3.0929e−5
238	−1.5190e−3	6.4356e−3	9.9960e−1	8.0261e−4
239	−6.6571e−3	2.5642e−2	9.9805e−1	3.4286e−3
240	−4.2300e−2	1.4481e−1	9.8627e−1	2.6585e−2
241	−1.2901e−1	3.8184e−1	9.5454e−1	1.0800e−1
242	−1.0720e+0	3.5970e−1		
243	−4.7146e−1	1.3388e−1		
244	−2.9469e−1	9.4322e−2		
246	−2.0295e+1	2.5009e+0		
248	−9.7199e+0	1.2012e+0		
250	−6.2588e+0	7.8924e−1		
254	−7.5734e+1	7.4988e+0		
256	−3.6815e+1	3.8225e+0		
258	−2.3882e+1	2.4879e+0		

The variances of the mean values are found by division of the tabulated variances by the number of configurations.

SPONTANEOUS ELECTRIFICATION OF ISOLATED CHARGED PORES

Since the two types of ions fluctuate as determined by their own bulk electrochemical potentials, there is no guarantee that the pore will in the average be uncharged, except when the pore is uncharged *and* the two ions have equal diameter *and* when the externally applied potential (Δ) is zero. We have calculated the *average electrification* of a pore as follows:

$$\text{Average electrification} = \langle EL \rangle = Q/e_0 + z_+\langle N_+ \rangle - |z_-|\langle N_- \rangle \qquad (15)$$

For the RPM, we have $\langle EL \rangle = (Q/e_0) + z\langle N_+ \rangle - z\langle N_- \rangle$. Performing simulations for the 1:1 electrolyte, the surface charge (Q/e_0) and the external potential $-\Delta$ yields the same results for $\langle N_+ \rangle$ and $\langle N_- \rangle$ as a simulation of a $z{:}z$ electrolyte with the same B and ρ^* and with the surface charge replaced by (zQ/e_0) and external potential by $-\Delta/z$. Thus, $\langle EL \rangle/z$ in the two cases have the same value.

In the case of *no external applied potential* ($\Delta = 0$) we shall call the electrification for *spontaneous electrification*. Table 5 in ref. [1] already seemed to indicate, that this electrification was a function solely of $\tau\kappa a$ (*i.e.* the radius of the accessible part of the pore scaled by the Debye length) quite independent of the Bjerrum parameter and the concentration of the bulk electro-lyte. However, this table only included 16 simulations with two values of B and 3 values of ρ^* and only one value of $Q/e_0 (=1)$.

In figures 1–2, the spontaneous electrification is shown as a function of $\tau\kappa a$ for $Q/e_0 = 0$, $Q/e_0 = 1$, $Q/e_0 = 5$ and $Q/e_0 = 10$. The values of R/a are running from 1 (extremely small pores) to 35 (quite spacy pores). Three different Bjerrum parameters (1.546, 1.681 and 2) corresponding to 1:1 electrolytes at 25°C in water are incorporated. In addition, a high Bjerrum parameter (6.8116) is incorporated corresponding to a (very dilute) 1:1 electrolyte at a low dielectric constant. Electrolyte concentrations from ultra-dilute to moderately concentrated are used in the simulations. For the three Bjerrum parameters, there is a common curve for each value of Q/e_0. The high Bjerrum parameter electrolyte exhibits some deviation at low values of $\tau\kappa a$, the more the higher is the surface charge. For the uncharged pores there is naturally no spontaneous electrification since the ions are identical apart from the charge (and possibly the mass, but this does not affect the present calculations). For the charged pores – which are all positively charged – the spontaneous electrification is seen always to be *positive*. For $\tau\kappa a \to 0$, the deviation from electroneutrality tends towards Q/e_0 (except for B = 6.8116). In the opposite extreme – for $\tau\kappa a \gg 1$ – the electrification tends to zero. What does this mean?

The statement $\tau\kappa a \to 0$ means one of two things: Either the pore radius tends to zero, and the probability of having either a cation or an anion tends to zero with a fixed external salt concentration. Then $\langle N_+ \rangle = \langle N_- \rangle = 0$, and the charge of the pore is the fixed charge Q/e_0. Alternatively, the bulk electrolyte concentration (and κ) tends to zero for a given radius. The occupation numbers will also tend to zero and the result is the same as above. Conversely, the statement $\tau\kappa a \to \infty$ means either that the pore radius grows large or that the bulk concentration is large. In the first case, the system tends toward a macroscopic system, and the electrostatic forces then tend to induce *electroneutrality* in the system – not only in a relative but also in absolute sense. In the second case, the high concentration of cations and anions inside the pore quenches any deviation from electroneutrality.

Why does the extremely dilute B = 6.8116 electrolyte deviate at small values of

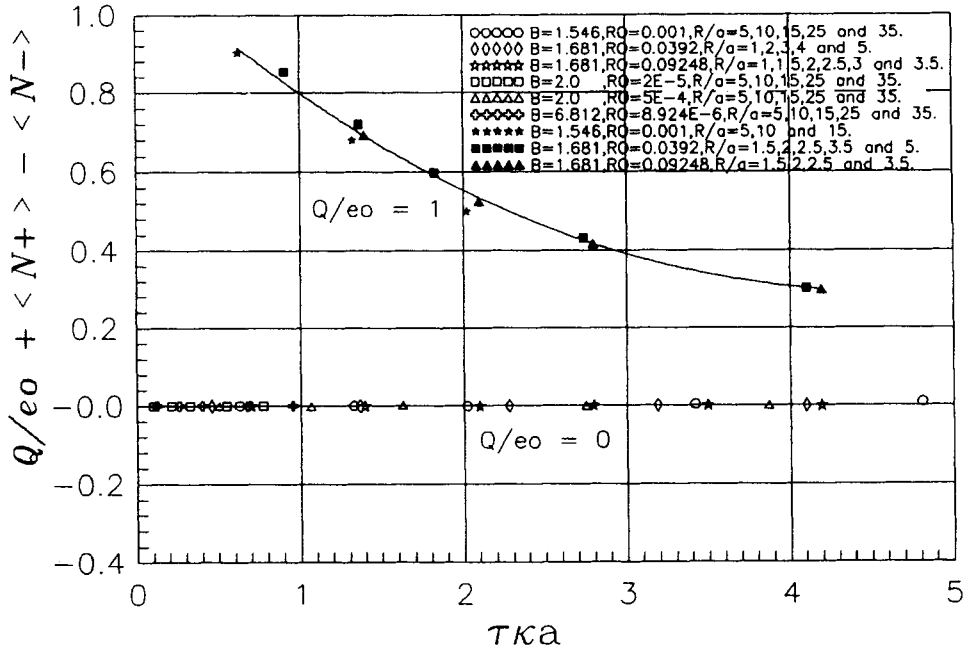

Figure 1 The spontaneous electrification of pores of many different radii (R/a from 1 to 35) with many different Bjerrum parameters ($B = 1.546$, 1.681, 2, 6.8116) and many different densities (ρ^* from $8.9 \cdot 10^{-1}$ to 0.092) is a function solely of the radius of the available pore scaled by the Debye length ($\tau\kappa a$) for a pore surface charge equal to unity ($Q/e_0 = 1$). For zero surface charge there is no electrification . For $\tau\kappa a \to 0$ (small pores or small concentrations) the spontaneous electrification tends towards Q/e_0. Symbols: $B = 1.546$, $\rho^* = 0.001$, $R/a = 5$, 10, 15, 25 *and* 35 (O); $B = 1.681$, $\rho^* = 0.0392$, $R/a = 1$, 2, 3, 4 and 5 (open diamonds); $B = 1.681$, $\rho^* = 0.09248$, $R/a = 1$, 1.5, 2, 2.5, 3 and 3.5 (open stars); $B = 2$, $\rho^* = 2 \cdot 10^{-5}$, $R/a = 5$, 10,15, 25 and 35 (□); $B = 2$, $\rho^* = 5 \cdot 10^{-4}$, $R/a = 5$, 10, 15, 25 and 35 (Δ); $B = 6.8116$, $\rho^* = 8.924 \cdot 10^{-6}$, $R/a = 5$, 10, 15, 25 *and* 35 (*open crosses*); $B = 1.546$, $\rho^* = 0.001$, $R/a = 5$, 10 and 15 (black stars); $B = 1.681$, $\rho^* = 0.0392$, $R/a = 1.5$, 2, 2.5, 3.5 and 5 (■); $B = 1.681$, $\rho^* = 0.09248$, $R/a = 1.5$, 2, 2.5 and 3.5 (▲).

$\tau\kappa a$? The curves tend towards lower values than Q/e_0. The reason is, that there is a quite strongly bound *contact adsorption layer* of anions close to the pore wall. In this region, the deviation from the simple, diffuse double layer behaviour is quite high. For small pores, these deviations dominate, and the scaling by the Debye length is not meaningful. Said in another way, the probability of having a cation in the pore decreases much faster with decreasing pore size than the probability of having an anion, and the spontaneous electrification is lowered compared to Q/e_0. The tendency is stronger for $Q/e_0 = 10$ than for $Q/e_0 = 5$, which is naturally explained, since the contact adsorption is greater in the former case.

It is of interest to note, that there is also a spontaneous electrification in the analytically solvable model for minimal pores, see appendix B. However, in that model no scaling with $\tau\kappa a$ exists. This is so, since the Debye length (and the double layer concept) has no meaning, when there can never be more than one ion at a

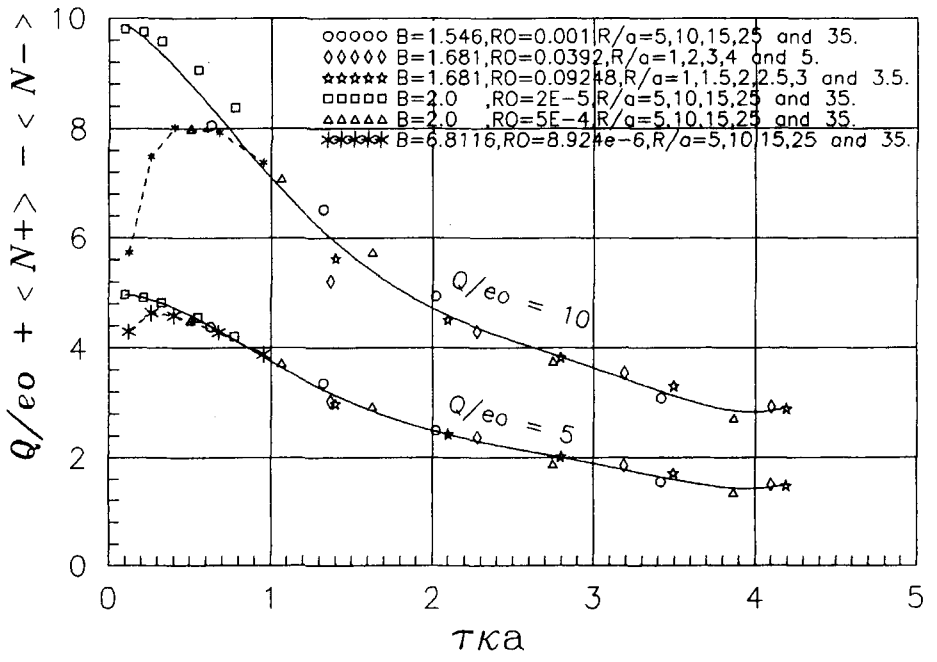

Figure 2 The spontaneous electrification for $Q/e_0 = 5$ and 10 for many different pore radii, Bjerrum parameters and densities as functions of $\tau\kappa a$. For $\tau\kappa a \to 0$ (small pores or small concentrations) the spontaneous electrification tends towards Q/e_0. However, deviations at low $\tau\kappa a$ - values from the common curves are seen for the very dilute electrolyte with $B = 6.8116$ and $\rho^* \approx 8.9 \cdot 10^{-6}$, especially at high surface charges. "Contact adsorption" of counterions in small pores makes the diffuse electric double layer description meaningless in small pores, when the Bjerrum parameter is high, and the extrapolated efficient surface charge less than Q/e_0. Symbols: $B = 1.546$, $\rho^* = 0.001$, $R/a = 5$, 10, 15, 25 and 35 (O); $B = 1.681$, $\rho^* = 0.0392$, $R/a = 1$, 2, 3, 4 and 5 (open diamonds); $B = 1.681$, $\rho^* = 0.09248$, $R/a = 1$, 1.5, 2, 2.5, 3 and 3.5 (open stars); $B = 2$, $\rho^* = 2 \cdot 10^{-5}$, $R/a = 5$, 10, 15, 25 and 35 (□); $B = 2$, $\rho^* = 5 \cdot 10^{-4}$, $R/a = 5$, 10, 15, 25 and 35 (Δ); $B = 6.8116$, $\rho^* = 8.924 \cdot 10^{-6}$, $R/a = 5$, 10, 15, 25 and 35 (*).

time in the pore. However, if there may be just some few ions at a time in the pore, the double layer is established and the Debye length has meaning. This is so, even if the *mean occupation numbers* of the ions are only tiny fractions of a single particle as in many of the simulations performed!

ELECTRIFICATION AS A FUNCTION OF APPLIED POTENTIAL

We shall now consider the effect of applying an electric potential difference Δ between the pore solution and the external solution. If we set the electric potential "very far away" from the pore in the ion free wall material equal to zero, we have the following dimensionless potential (η) everywhere *inside* the pore *before* any ions enter:

$$\eta = e_0\Psi(\text{inside, ion free})/kT = (Q/e_0)(B_r)(a/R)$$
$$= (B/z^2)(Q/e_0)/(\tau + 1/2) \qquad (16)$$

This is also a kind of applied potential. Even further away from the pore than "very far away", there is an interface towards the bulk solution. Passing through that interface the dimensionless potential jumps from zero to $-\Delta$. Thus, the *total applied potential* (pore minus bulk) is the sum of Δ and the potential from the pore surface charge:

$$\zeta = \text{Total dimensionless applied potential} = \Delta + \eta \qquad (17)$$

(It is seen, that the total applied potential has to be divided by z to have z-invariance of the results).

For pores with $R/a = 5$, the electrification is plotted as a function of the total applied potential (dimensionless) in Figure 3. The three curves are for the surface charges 1, 5 and 10 elementary charges. On each curve the points correspond from left to right to the values $\Delta = 0$, 2, 4, 6, and 8. The electrolyte has $B = 1.546$ and $\rho^* = 0.001$ ($\kappa a \approx 0.1394$). For increasing external potential, the positive electrification diminishes. This is clear, since it becomes energetically more favorable for the anion to enter the pore and at the same time less favorable for the cation, when the pore potential increases. At a certain value of Δ *electroneutrality* is obtained

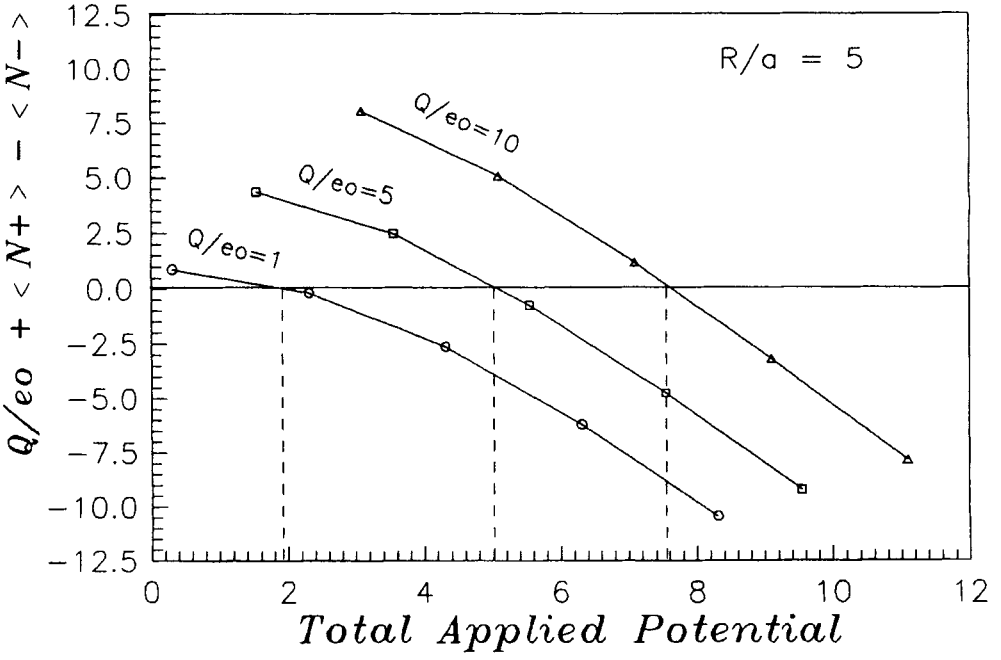

Figure 3 The dependence of the electrification on the total dimensionless applied potential ($\zeta = \Delta + \eta$) for three different surface charges for an alveolear radius equal to 5 times the ion diameter. $B = 1.546$, $Q^* = 0.001$. The points from left to right on each curve are for $\Delta = 0$, 2, 4, 6 and 8. The vertical dashed lines indicate values of $\zeta_{\text{Donnan}} = \Delta_{\text{Donnan}} + \eta$, where Δ_{Donnan} is the dimensionless Donnan potential.

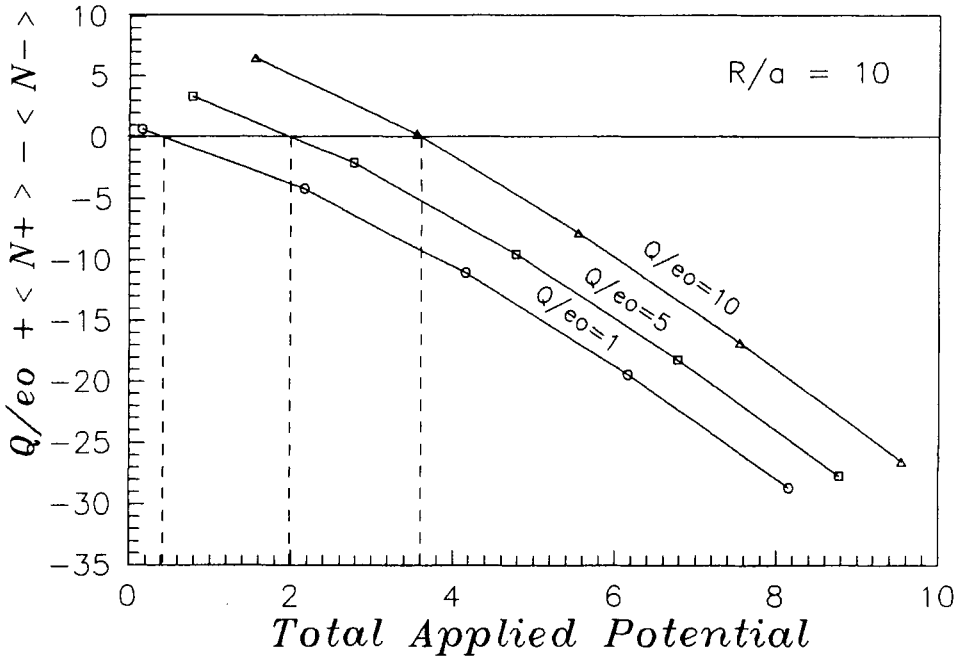

Figure 4 Same as Figure 3, but with $R/a = 10$.

(dashed vertical lines). These values correspond to the *Donnan potential* to which we shall return in the next section.

For the same electrolyte, but with $R/a = 10$ and $R/a = 15$, similar plots are shown in Figures 4–5. In Figure 6, the three triplet curves correspond to $Q/e_0 = 1$, 5 and 10 and in each triplet, the three curves are for $R/a = 5$, 10 and 15. The total applied potential here takes on small values, since the values of Δ have been chosen as negative. At zero total applied potential, the three curves in a triplet for a common surface charge coincide in Q/e_0. This is easily explained: When there is no total applied potential in the pore, the potential in the pore is the same as in the bulk (before any ions enter). Since the ions are identical - except for the charge - the average population numbers must be the same (but not zero this time!). Thus, the average electrification will be Q/e_0 following Eqn. (15).

The curves in Figure 6 corresponding to $R/a = 5$ (small pores) exhibit a slight dependence only on the total applied potential. For very small pores, the population numbers would always be zero without regard to applied potential, and the curve of electrification *vs.* applied potential would be flat. For somewhat larger pores, space restrictions still make it difficult to change the population numbers, and the slopes of the electrification curves have low values. The population numbers in large pores ($R/a = 15$) are very sensitive to applied potential, and the curves are steep.

The finding, that the electrification for small pores changes only slightly with total applied potential is supported by the behaviour of the minimal pore model (appendix B), where the electrification can only change from Q/e_0 to $Q/e_0 - z$ for any

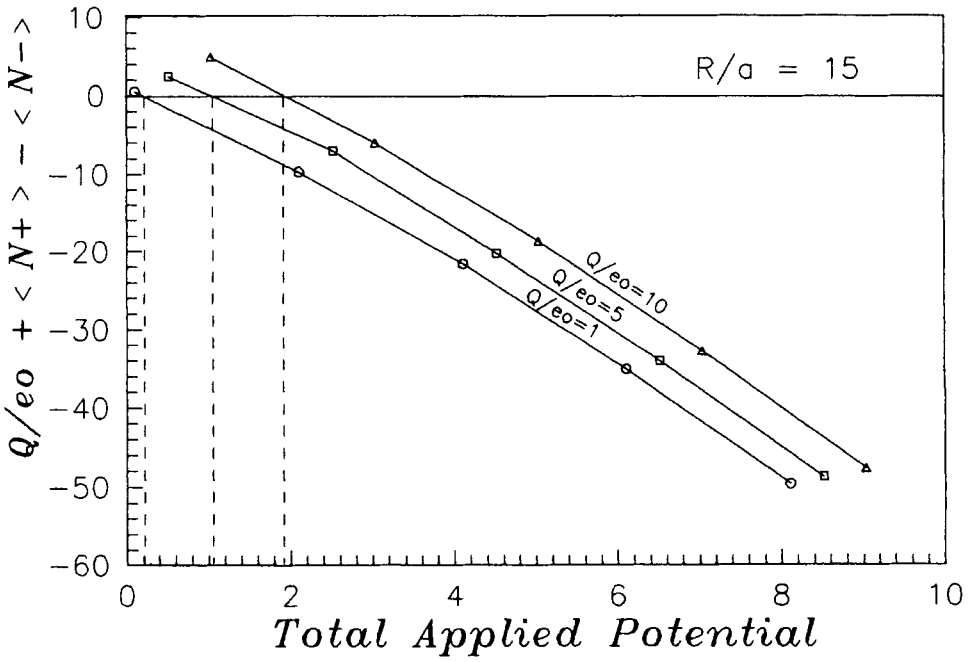

Figure 5 Same as Figure 3, but with $R/a = 15$.

$z{:}z$ electrolyte, when ζ passes from zero to infinity (from Q/e_0 to $Q/e_0 + z$, when ζ passes from zero to minus infinity). This means however, that Donnan potentials for such pores do only exist, when $z > abs(Q/e_0)$. Some consequences of this for *e.g.* small pore zeolithe minerals are discussed in appendix B.

PRECISE DETERMINATION OF DONNAN POTENTIALS

For B = 1.546, $\rho^* = 0.001$, $Q/e_0 = 5$ and $R/a = 5$, Figure 7 shows a precise determination of the Donnan potential, using a lot of simulations near electroneutrality and fitting the points with the most significant least square polynomial. The uncertainty in the Donnan potential is determined by the width of the uncertainty belt of the polynomial. The same has been done for a number of different $z{:}z$ electrolytes, pore sizes and surface charges. The final results are listed in Table 4. The values of Δ (Donnan, GCEMC) are here compared to the ideal values with all bulk and pore activity coefficients equal to unity.

If we equate the electrochemical potential of the cation in the bulk and in the pore, we obtain:

$$\ln[\langle N_+\rangle_{\text{pore}}/\{\rho^*{}_+(\text{bulk})(4\pi/3)\tau^3\}] + \ln[y_+(\text{pore})/y_+(\text{bulk})] + z\Delta = 0 \quad (18)$$

This equation implies the following definition of the *average single ion activity coefficient in the pore*: The ion activity in the pore is equal to the average single

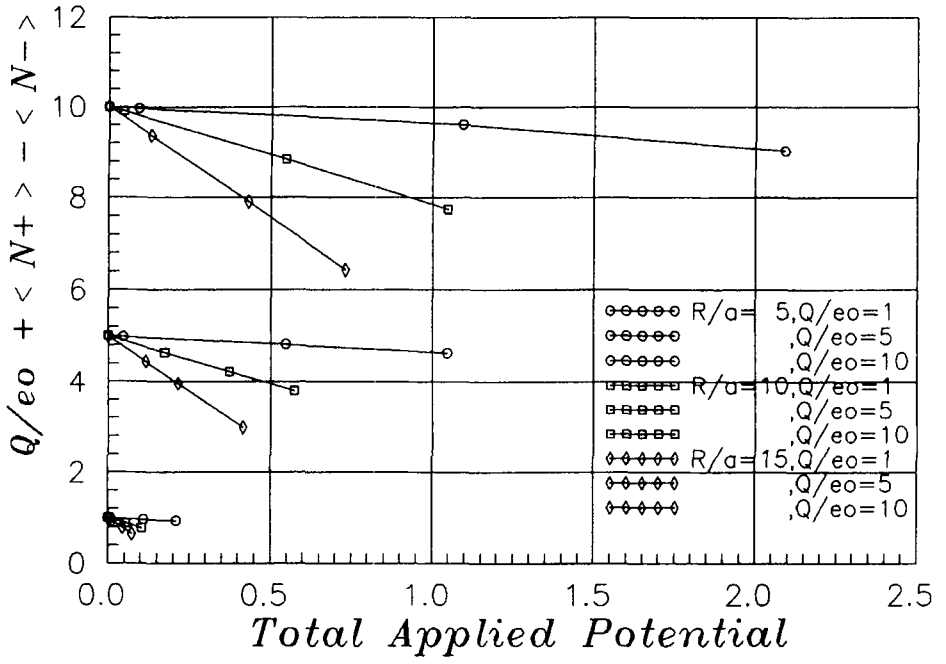

Figure 6 Same as Figures 3-5, but with total applied potentials tending towards zero (negative values of Δ). At zero total applied potential, we have $\langle N_+ \rangle = \langle N_- \rangle$, and the electricifaction becomes Q/e_0. The large alveoles have a more pronounced variation in the electrification with total applied potential than the small alveoles.

ion activity times the average density of the ion in the pore in the part of the pore *accessible* to the ion. Similarly for the anion:

$$\ln[\langle N_- \rangle_{\text{pore}}/\{\rho^*_-(\text{bulk})(4\pi/3)\tau^3\}] + \ln[y_-(\text{pore})/y_-(\text{bulk})] - z\Delta = 0 \tag{19}$$

Adding the two Equations (18-19) we obtain:

$$y_\pm(\text{pore})/y_\pm(\text{bulk}) = \langle N_\pm \rangle_{\text{bulk}}/\langle N_\pm \rangle_{\text{pore}} \tag{20}$$

with

$$\langle N_\pm \rangle_{\text{bulk}} = (4\pi/3)\tau^3(\rho^*/2) \tag{21}$$

$$\langle N_\pm \rangle_{\text{pore}} = \sqrt{[\langle N_+ \rangle_{\text{pore}}\langle N_- \rangle_{\text{pore}}]} \tag{22}$$

Thus, the *average mean ionic activity coefficient in the pore* defined by

$$y_\pm(\text{pore}) = \sqrt{[y_+(\text{pore})y_-(\text{pore})]} \tag{23}$$

may be calculated from the occupation numbers and from the mean ionic activity coefficient in the bulk phase. Even if it may seem, that all potential dependence was eliminated with Δ by the addition of Equations (18-19), we shall see later, that this is *not* the case, since the average activity coefficients in small pores are themselves dependent on the applied potential!

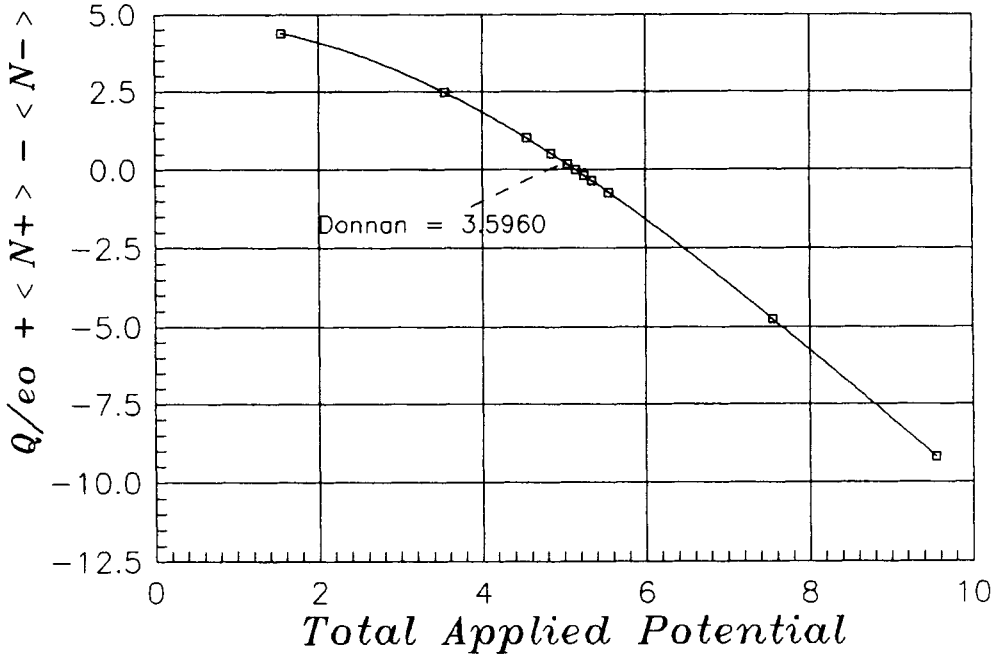

Figure 7 Precise determination of the dimensionless Donnan potential (Δ_{Donnan}) for an alveole with $R/a = 5$ and $Q/e_0 = 5$ with an RPM electrolyte with $\rho^* = 0.001$ and $B = 1.546$. The electrification of the alveole is zero at Δ_{Donnan}. The horizontal axis is $\zeta = \Delta + \eta$.

Alternatively we obtain from Equations (18-19):

$$\langle N_+ \rangle_{pore} / \langle N_\pm \rangle_{bulk} = [y_+(\text{bulk})/y_+(\text{pore})] \exp(-z\Delta) \tag{24}$$

$$\langle N_- \rangle_{pore} / \langle N_\pm \rangle_{bulk} = [y_-(\text{bulk})/y_-(\text{pore})] \exp(z\Delta) \tag{25}$$

Introducing the quantities

$$\alpha = \exp(z\Delta) \tag{26}$$

$$Q^* = [\langle N_+ \rangle_{pore} - \langle N_- \rangle_{pore}] / \langle N_\pm \rangle_{bulk} \tag{27}$$

we obtain a second degree expression in α:

$$[y_-(\text{bulk})/y_-(\text{pore})]\alpha^2 + Q^*\alpha - [y_+(\text{bulk})/y_+(\text{pore})] = 0 \tag{28}$$

If we also require *overall electroneutrality* in the pore, we have $Q^* = -Q/[e_0 z \langle N_\pm \rangle_{bulk}]$ and the positive root $\alpha = \alpha_D$ corresponds to the non-ideal *Donnan potential.* In the case where all activity coefficients may be taken equal to unity (dilution ideality) or in the case, where the activity coefficients of the same kind of ion are equal in the bulk and in the pore solution, we obtain:

$$\alpha_D^2 - Q/[e_0 z \langle N_\pm \rangle_{bulk}]\alpha_D - 1 = 0 \tag{29}$$

This equation is nothing but a special case of an (ideal) *Donnan polynomial* such as discussed for arbitrary electrolyte mixtures in ion exchange membranes in reference [12]. Equation (29) is the equation used for calculating the *ideal Donnan*

potentials in Table 4. It is seen, that the Donnan potential - as expected - is deviating only few per cent from the ideal value in the case of very dilute solutions, even for the high Bjerrum parameter $B = 6.8116$ (1:1 electrolyte at low dielectric constant). At higher concentrations the deviations are more pronounced. It is interesting to observe, that small pores have generally the least deviation from the ideal Donnan potential. The reason might be, that the interactions between the ions in small pores are quite small, since the ions are most often alone in the pores. At the same pore size and electrolyte concentration, the deviation from the Donnan potential most often increases with increasing surface charge Q/e_0 as expected, but this is not always the case and any easy explanation cannot be offered.

MEAN IONIC OCCUPATION NUMBERS AND THEIR DEPENDENCE ON TOTAL APPLIED POTENTIAL

The *mean ionic occupation number* in the pore is defined by Equation (22). In Figures 8a–c, the dependence on the total applied potential of the quantity $\langle N_\pm \rangle_{\text{pore}}/\langle N_\pm \rangle_{\text{bulk}}$ is shown. For the same pore size there is only one curve for different values of Q/e_0 and of Δ. The mean ionic occupation numbers are always increasing with increasing total applied potential, but the relative increase is larger for the small pores than for the large. This is understandable, since a very large pore is almost as a bulk solution, and in such solution an applied electric potential has no importance for the chemical potential of an electroneutral electrolyte. Another way to say this is to observe that the factors $\exp(\pm z\Delta)$ cancel, when Equations (24) and (25) are multiplied together, and for large pores, the activity coefficients will not depend on the potential. The increase with the total applied potential of $\langle N_\pm \rangle_{\text{pore}}$ in the case of small pores we shall briefly call the phenomenon of *electrosorption*. This phenomenon must be linked to the existence of the diffuse double layer, since for the minimal pore model - where no double layer exists - the value of $\langle N_\pm \rangle_{\text{pore}}$ *decreases* with increasing Δ, see appendix B.

AVERAGE MEAN IONIC AND SINGLE ION ACTIVITY COEFFICIENTS IN PORES

The mean ionic occupation numbers may be translated to average mean ionic activity coefficients in pores by means of Equation (20). Figure 9 shows the ratio $y_\pm(\text{pore})/y_\pm(\text{bulk})$ as a function of the total applied potential for an electrolyte with $B = 1.546$ and $\rho^* = 0.001$. For each pore size, there is one single curve irrespective of the values of Q/e_0 (being 0, 1, 5 or 10) or Δ (being 0, 2, 4, 6 and 8). At zero total applied potential, the smallest pore ($R/a = 5$) has the highest value of $y_\pm(\text{pore})$, *i.e.* 7% above the bulk value. This is due to the space restrictions. For $R/a = 10$ the pore activity coefficient is 4% higher and for $R/a = 15$, 2.5% higher than the bulk value.

The values of $y_\pm(\text{pore})/y_\pm(\text{bulk})$ *decreases* with increasing total applied potential (electrosorption). The decrease is the greater the smaller is the pore. (However, when the pore is a minimal pore ($1/2 < R/a < 1$) the behaviour is radically different with an exponential *increase* in $y_\pm(\text{pore})$ for high values of ζ, see appendix B, Equations B17–B18).

Table 4 Ideal, non-ideal Donnan potentials and percentage of deviation for electroneutral pores.

No.	$\Delta_D(GCMC)$	$\Delta_D(ideal)$	*% Deviation*
67	1.806	1.6908	6.39
77	0.3245	0.2749	15.3
87	0.1035	0.0782	24.5
101	3.596	3.2671	9.14
113	1.328	1.1334	14.6
123	0.5032	0.3821	24.1
137	4.572	3.9592	13.4
146	2.078	1.7479	15.9
155	0.9480	0.7194	24.1
194	5.603	5.5682	0.614
195	3.366	3.3279	1.14
196	2.112	2.0739	1.82
198	7.443	7.1777	3.57
200	5.083	4.9361	2.89
202	3.781	3.6681	2.99
206	8.462	7.8708	6.99
208	5.922	5.6292	4.95
210	4.573	4.3608	4.64
218	2.469	2.3583	4.49
219	0.603	0.5315	11.8
220	0.1931	0.1559	19.2
222	4.304	3.9792	8.01
224	1.973	1.7479	11.4
226	0.8783	0.7194	18.1
230	5.321	4.6520	12.6
232	2.790	2.4183	13.3
234	1.511	1.2309	18.5
242	6.170	6.3752	−3.33
243	4.161	4.1338	0.664
244	2.947	2.8682	2.67
246	8.026	7.9847	0.510
248	5.895	5.7430	2.58
250	4.661	4.4746	4.01
254	9.132	8.6778	4.97
256	6.800	6.4362	5.35
258	5.532	5.1676	6.58

% deviation = $[(\Delta_D(GCMC) - \Delta_D(ideal))/\Delta_D(GCMC)] \cdot 100$
The uncertainty on $\Delta_D(GCMC)$ is on the last digit.

In a very large pore, the conditions are almost as in the bulk solution, where the applied potential has no influence on $y_\pm$, and the curve should approach the horizontal line $y_\pm(\text{pore})/y_\pm(\text{bulk}) = 1$. Therefore, the curve for the small pore ($R/a = 5$) crosses the curves for the larger pores ($R/a = 10$ and 15) as shown in Figure 9.

The average single ion activity coefficients in the pores may also be calculated. The Equation (28) may be used to find the non-ideal Donnan potential, if $Q^* = -Q/[e_0 z\langle N_\pm\rangle_{bulk}]$ and if the single ion activity coefficients in the pores were known. The latter is not the case. By the GCEMC simulations, we have rather determined the Donnan potential as the external potential leading to overall pore electroneutrality. Then, Equation (28) may be used the other way round to calculate the single ion activity coefficients. Incidentally, we can perform this calculation even

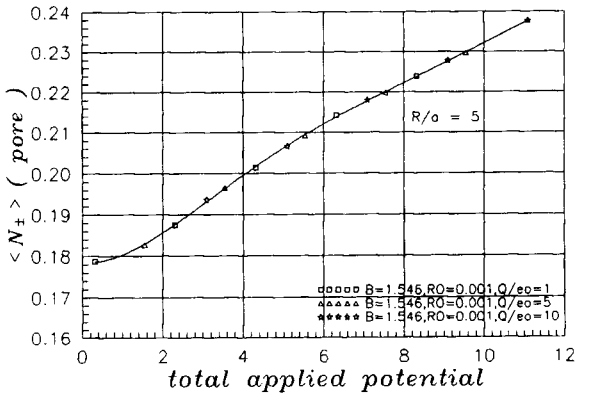

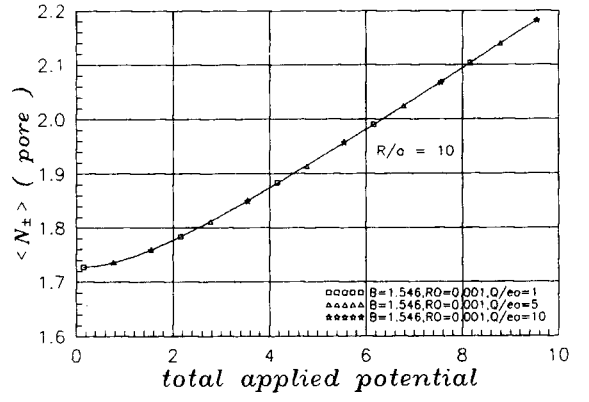

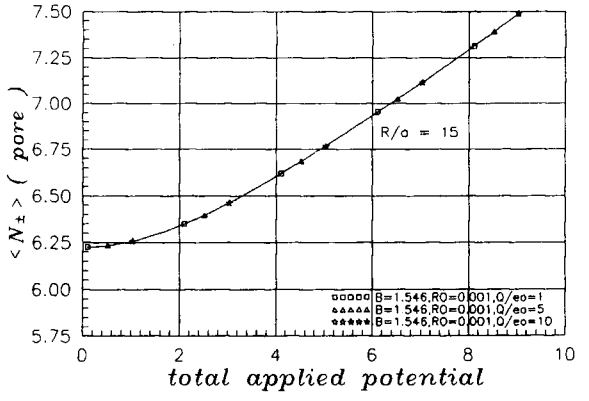

Figures 8 a–c The geometric mean of the ion population numbers in alveoles with sizes $R/a = 5$ (Figure 8a), $R/a = 10$ (Figure 8b) and $R/a = 15$ (Figure 8c) as a function of the dimensionless total applied potential (η). The increase in $\langle N_{\pm} \rangle$ with increasing η is called electrosorption. The relative increase is larger for smaller pores.

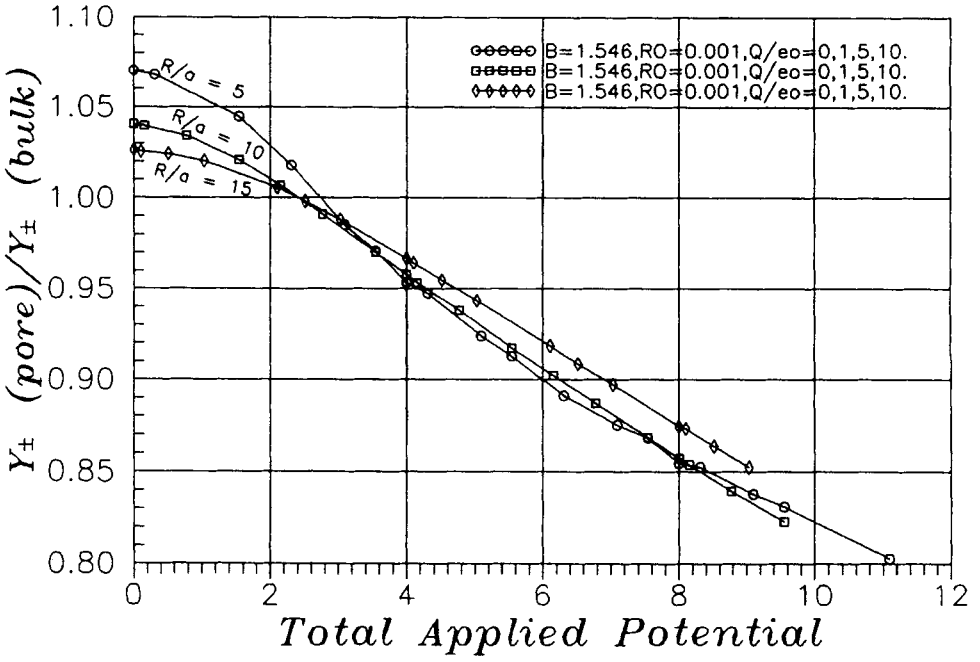

Figure 9 Calculated average values of the mean ionic activity coefficients in the pores relative to the bulk value of the mean ion activity coefficient *vs.* η for different pore radii and pore charges. The RPM electrolyte has $B = 1.546$ and $\rho^* = 0.001$. (For this electrolyte we have $y_{\pm}(\text{bulk}) = 0.9082$, see reference 10, Table 1).

in situations, where the potential differs from the Donnan potential, and where there is not overall electroneutrality in the pore. For the RPM we have: $y_+(\text{bulk}) = y_-(\text{bulk}) = y_{\pm}(\text{bulk})$. Inserting this into Equation (28), and using also Equation (23) for $y_{\pm}(\text{pore})$, we obtain:

$$\exp(2z\Delta)\,[y_{\pm}(\text{bulk})/y_{\pm}(\text{pore})]x^2 + Q^* \exp(z\Delta)x - [y_{\pm}(\text{bulk})/y_{\pm}(\text{pore})] = 0 \quad (30)$$

$$x = [y_+(\text{pore})/y_{\pm}(\text{pore})] \quad (31)$$

Thus, knowing the applied potential Δ, $y_{\pm}(\text{bulk})/y_{\pm}(\text{pore})$ and Q^* from Equation (27), we may find $x = y_+(\text{pore})/y_{\pm}(\text{pore})$ as the positive root of the second degree equation (30). This ratio is plotted against Q/e_0 for several pore sizes in Figure 10. The electrolyte is $(B, \rho^*) = (1.546, 0.001)$ and the external potential is $\Delta = 0$. The increase in the single ion activity coefficient in the pore relative to $y_{\pm}(\text{pore})$ with the increasing potential from the surface charge is very dramatic for the smallest pore ($R/a = 5$). In the large pore, the ratio $y_+(\text{pore})/y_{\pm}(\text{pore})$ is more near to unity like it would be in a bulk solution of a RPM electrolyte. The curves for all pore sizes start with the value 1 for $Q/e_0 = 0$. Since $\Delta = 0$, the total applied potential in the pore is here = 0, and the two ions only "feel" identical space restrictions, so that their single ion activity coefficients are equal to each other and equal to $y_{\pm}(\text{pore})$ like in the bulk solution. (However, $y_{\pm}(\text{pore}) > y_{\pm}(\text{bulk})$ at zero total applied potential, see Figure 9).

In Figure 11, the ratio $y_-(\text{pore})/y_\pm(\text{pore})$ is plotted against Q/e_0 for the same situations as in Figure 10. In the small pore, there is now a dramatic decrease in this ratio with increasing surface charge. Figure 12 exhibits the variations in $y_+(\text{pore})/y_\pm(\text{pore})$ for the same electrolyte at an applied potential $\Delta = 4$. Now, the total applied potential is *not* zero at $Q/e_0 = 0$, and the curves do not start from unity at this value. Still the smallest pore exhibit the most dramatic variation of $y_+(\text{pore})/y_\pm(\text{pore})$ with Q/e_0, but it is relatively much less than in the case of $\Delta = 0$. In Table 5, the values of the average pore activity coefficients are listed for the GCEMC simulations performed at the Donnan potentials.

EXCESS ENERGY AND OTHER AVERAGES

The *excess energy* (electrostatic energy) for the pore ions has also been sampled. In Table 3, the dimensionless excess energies $E_{ex}/kT = \langle U/kT \rangle$ and the values of $\langle \exp(U/kT) \rangle$ were listed together with the *variances of the individual samplings* of these quantities. From $\text{VAR}(U/kT)$ it is possible to calculate the *uncertainty* of the grand canonical average E_{ex}/kT as $\sqrt{[\text{VAR}(U/kT)/\text{total number of configurations}]}$. Furthermore, it is possible to calculate a quantity related to the excess heat capacity from $\text{VAR}(U/kT)$. For a one component system, Hill has shown the

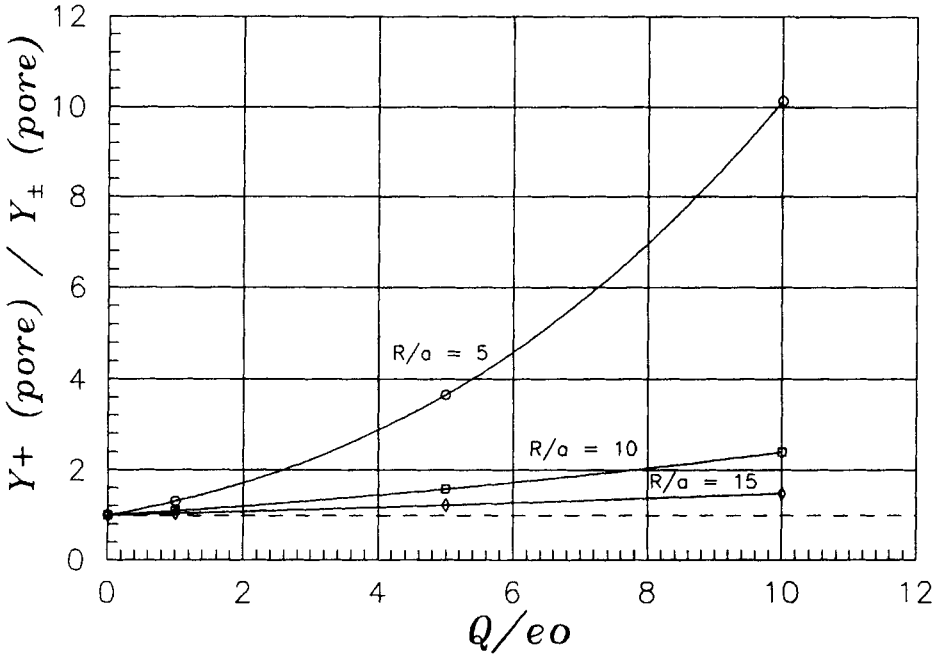

Figure 10 The average value of the *single ion* activity coefficient for the cation in the pores relative to the value of $y_\pm(\text{pore})$ for the same electrolyte and pores as in Figure 9. There is a drastic increase in $y_+(\text{pore})/y_\pm(\text{pore})$ with the surface charge (applied potential) for small pores. The dashed horizontal line indicates the bulk limit (large pores), where the ratio is always unity for an RPM electrolyte. (The dimensionless potential $\Delta = 0$).

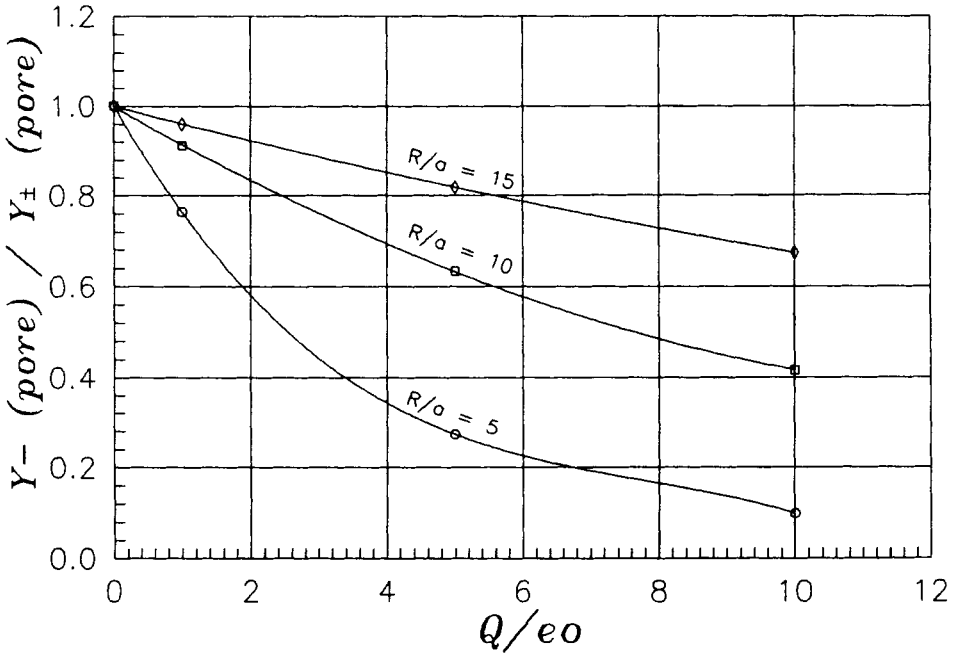

Figure 11 The average value of the *single ion* activity coefficient for the anion in the pores relative to the value of $y_{\pm}$(pore) for the same electrolyte and pores as in Figure 10. There is an asymptotic decrease towards zero in y_{-}(pore)/$y_{\pm}$(pore) with increasing surface charge (applied potential) for small pores. (The dimensionless potential $\Delta = 0$).

following relations to be valid for a grand canonical ensemble with one fluctuating component [14]:

$$\mathrm{VAR}(J/kT) = C_{\mu,V}/k \tag{32}$$

J is the instantaneous value of the *heat function* corresponding to a one component grand canonical ensemble

$$J = \varepsilon - \mu N \tag{33}$$

$C_{\mu,V}/k$ is the total heat capacity at constant volume and constant chemical potential, and ε is the instantaneous total energy $U_{\mathrm{kin}} + U$. Hill shows that

$$\mathrm{VAR}(\varepsilon/kT) = (C_{\mu,V}/k) + 2(\mu/k)(\partial\langle N\rangle/\partial T)_{\mu,V} + (\mu^2/kT)(\partial\langle N\rangle/\partial\mu)_{T,V} \tag{34}$$

We have:

$$C_{\mu,V} = C_{N,V} + (\partial\langle N\rangle/\partial T)_{\mu,V}[(\partial\langle\varepsilon\rangle/\partial\langle N\rangle)_{T,V} - \mu] \tag{35}$$

Using also

$$\begin{aligned}(\partial\langle\varepsilon\rangle/\partial\langle N\rangle)_{T,V} &= \mu + T(\partial S/\partial\langle N\rangle)_{T,V} \\ &= \mu + T[(\partial\langle N\rangle/\partial T)_{\mu,V})/(\partial\langle N\rangle/\partial\mu)_{T,V}]\end{aligned} \tag{36}$$

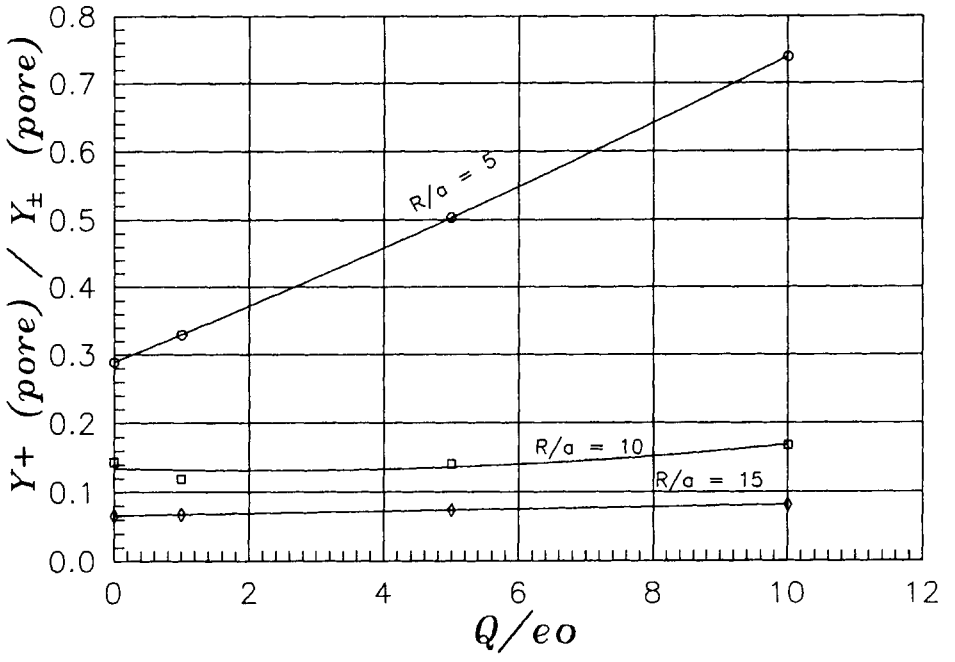

Figure 12 Same as Figure 10 but with the dimensionless applied potential $\Delta = 4$. Now, the ratio $y_+(\text{pore})/y_\pm(\text{pore})$ is *not* equal to unity for $Q/e_0 = 0$, since the values of $\langle N_+ \rangle$ and $\langle N_- \rangle$ are *not* identical for chargeless pores, when $\Delta \neq 0$.

we have finally:

$$\text{VAR}(\varepsilon/kT) = (C_{N,V}/k) + [\mu(\partial\langle N\rangle/\partial\mu)_{T,V}) + T(\partial\langle N\rangle/\partial T)_{\mu,V}]^2/[T(\partial\langle N\rangle/\partial\mu)_{T,V}] \quad (37)$$

From this equation, it is evident, that the variance of ε/kT is *not* simply $C_{N,V}/k$ as in a canonical ensemble, but has a *larger* value due to the number fluctuation term. In the argumentation of Hill, nothing is used which excludes the use of (37) on a *heterogeneous* systems such as a pore of finite size. However, in the present case we have *two* fluctuating species. Repeating all of Hill's derivations with the function

$$K = \varepsilon - \mu_{+,\text{el}}N_+ - \mu_{-,\text{el}}N_- \quad (38)$$

instead of (33), we arrive at the equations:

$$\text{VAR}(K/kT) = C_{\mu\text{el},V}/k \quad (39)$$

$$C_{\mu\text{el},V} = C_{N,V} + \sum_i (\partial\langle N_i\rangle/\partial T)_{\mu\text{el},V}[(\partial\langle\varepsilon\rangle/\partial\langle N_i\rangle)_{T,V,\mu j\neq i,\text{el}} - \mu_{i,\text{el}}] \quad (40)$$

$$\text{VAR}(\varepsilon/kT) = C_{N,V}/k + \text{CORR} \quad (41)$$

Table 5 Average mean ionic and single ion activity coefficients at the Donnan potentials.

No.	*B*	κa	Q/e_0	R/a	$Y_{\pm}(pore)$	$Y_{+}(pore)$	$Y_{-}(pore)$
51	1.546	0.1393	0	5	0.9724	0.9727	0.9722
54	1.546	0.1393	0	10	0.9438	0.9440	0.9437
57	1.546	0.1393	0	15	0.9318	0.9318	0.9318
60	1.546	0.1393	0	25	0.9226	0.9225	0.9227
61	1.546	0.1393	0	35	0.9196	0.9196	0.9196
67	1.546	0.1393	1	5	0.9295	0.8464	1.0207
77	1.546	0.1393	1	10	0.9418	0.9056	0.9795
87	1.546	0.1393	1	15	0.9315	0.9101	0.9534
101	1.546	0.1393	5	5	0.8360	0.5545	1.2606
113	1.546	0.1393	5	10	0.9157	0.7587	1.1053
123	1.546	0.1393	5	15	0.9268	0.8273	1.0383
137	1.546	0.1393	10	5	0.7815	0.3644	1.6758
146	1.546	0.1393	10	10	0.8788	0.6128	1.2604
155	1.546	0.1393	10	15	0.9157	0.7324	1.1448
189	2.0	0.0224	0	5	0.9741	0.9722	0.9760
190	2.0	0.0224	0	10	0.9775	0.9777	0.9773
191	2.0	0.0224	0	15	0.9767	0.9787	0.9747
192	2.0	0.0224	0	25	0.9918	0.9918	0.9919
193	2.0	0.0224	0	35	0.9898	0.9900	0.9897
194	2.0	0.0224	1	5	0.9181	0.8328	1.0121
195	2.0	0.0224	1	10	0.9642	0.9142	1.0169
196	2.0	0.0224	1	15	0.9815	0.9488	1.0154
198	2.0	0.0224	5	5	0.7333	0.4216	1.2753
200	2.0	0.0224	5	10	0.8997	0.7145	1.1329
202	2.0	0.0224	5	15	0.9355	0.7989	1.0954
206	2.0	0.0224	10	5	0.6057	0.2076	1.7667
208	2.0	0.0224	10	10	0.8161	0.5079	1.3114
210	2.0	0.0224	10	15	0.8959	0.6637	1.2094
213	2.0	0.1120	0	5	0.9728	0.9715	0.9740
214	2.0	0.1120	0	10	0.9452	0.9456	0.9447
215	2.0	0.1120	0	15	0.9297	0.9295	0.9299
216	2.0	0.1120	0	25	0.9181	0.9181	0.9182
217	2.0	0.1120	0	35	0.9131	0.9131	0.9132
218	2.0	0.1120	1	5	0.8886	0.7817	1.0102
219	2.0	0.1120	1	10	0.9384	0.8898	0.9895
220	2.0	0.1120	1	15	0.9297	0.9003	0.9601
222	2.0	0.1120	5	5	0.7469	0.4374	1.2754
224	2.0	0.1120	5	10	0.8789	0.6843	1.1289
226	2.0	0.1120	5	15	0.9148	0.7855	1.0653
230	2.0	0.1120	10	5	0.6727	0.2565	1.7641
232	2.0	0.1120	10	10	0.8229	0.5174	1.3088
234	2.0	0.1120	10	15	0.8881	0.6612	1.1928
237	6.811	0.0276	0	5	0.9876	0.9876	0.9876
238	6.811	0.0276	0	10	0.9764	0.9747	0.9782
239	6.811	0.0276	0	15	0.9633	0.9631	0.9635
240	6.811	0.0276	0	25	0.9495	0.9495	0.9495
241	6.811	0.0276	0	35	0.9388	0.9387	0.9389
242	6.811	0.0276	1	5	0.3022	0.1246	0.7329
243	6.811	0.0276	1	10	0.6008	0.3906	0.9242
244	6.811	0.0276	1	15	0.7762	0.6181	0.9747
246	6.811	0.0276	5	5	0.1294	0.01785	0.9386
248	6.811	0.0276	5	10	0.3367	0.1080	1.0490
250	6.811	0.0276	5	15	0.5161	0.2453	1.0859
254	6.811	0.0276	10	5	0.08760	0.005408	1.4188
256	6.811	0.0276	10	10	0.2498	0.04819	1.2957
258	6.811	0.0276	10	15	0.4002	0.1237	1.2949

$$\begin{aligned}\mathrm{CORR} \equiv\ & (1/k)\sum_i (\partial N_i/\partial T)_{\mu_{\mathrm{el}},V}[T(\partial S/\partial N_i)_{T,V,N_{j\neq i}}] \\ & + (2/k)\sum_i \mu_{i,\mathrm{el}}(\partial N_i/\partial T)_{\mu_{\mathrm{el}},V} \\ & - (\mu_{\mathrm{salt}}/kT)\sum_i \mu_{i,\mathrm{el}}(\partial N_i/\partial \mu_{i,\mathrm{el}})_{\mu j\neq i,\mathrm{el},V,T} \end{aligned} \tag{42}$$

or (using the electroneutrality in the T derivatives and transforming the partial ionic excess entropies):

$$\begin{aligned}\mathrm{CORR} =\ & (T/k)(\partial N_{\mathrm{salt}}/\partial T)^2_{\mu_{\mathrm{salt}},V}[(\partial\mu_{\mathrm{salt}}/\partial N_+)_{T,VN_-} + (\partial\mu_{\mathrm{salt}}/\partial N_-)_{T,VN_+}] \\ & + 2(\mu_{\mathrm{salt}}/k)(\partial N_{\mathrm{salt}}/\partial T)_{\mu_{\mathrm{salt}},V} - (\mu_{\mathrm{salt}}/kT)\mu_{+,\mathrm{el}}(\partial N_+/\partial\mu_{+,\mathrm{el}})_{T,V\mu_-,\mathrm{el}} \\ & - (\mu_{\mathrm{salt}}/kT)\mu_{-,\mathrm{el}}(\partial N_-/\partial\mu_-)_{T,V\mu_+,\mathrm{el}} \end{aligned} \tag{43}$$

We have not been able to bring the latter correction term to a "smart" form showing directly its positive sign, but physical reasoning indicates that it should be positive just as for a single fluctuating component. It should be noticed, that $\mathrm{VAR}(\varepsilon/kT) = \mathrm{VAR}(\varepsilon_{\mathrm{kin}}/kT) + \mathrm{VAR}(U/kT)$ since there is no correlation between kinetic and potential energy. The first term is the kinetic contribution to $C_{\mu_{\mathrm{el}},V}$, the second the excess contribution.

We now turn to the significance of the average $\langle \exp(U/kT)\rangle$. This quantity only has a clear physical meaning in the limit $\tau \to \infty$, however. In this case the pore becomes a macroscopic system and the *relative* fluctuations in number are small. Then, the *maximum term method* may be applied. In this limit we have (see reference 14, sect. 20):

$$\Xi \to \exp(N^*_+\mu_{+,\mathrm{el}} + N^*_-\mu_{-,\mathrm{el}})Q(N^*_+, N^*_-) \tag{44}$$

where $Q(N^*_+, N^*_-)$ is the *canonical* partition function evaluated using the *most probable* occupation numbers of the ions. Thus, for the grand canonical average of the *electrostatic energy* $\exp(U/kT)$ we have in the bulk limit:

$$\begin{aligned}&\langle \exp(U/kT)\rangle = \\ &\Xi^{-1}\sum_{N_+,N_-}(\Lambda_+)^{-3N_+}(\Lambda_-)^{-3N_-}\exp\left(\sum N_i\mu_{i,\mathrm{el}}\Big/kT\right)\exp(U/kT)\int\exp(-U_{\mathrm{tot}}/kT)\,\mathrm{d}\mathbf{r}_{N_+}\,\mathrm{d}\mathbf{r}_{N_-} \\ &\to \Xi^{-1}(\Lambda_+)^{-3N^*_+}(\Lambda_-)^{-3N^*_-}\exp\left(\sum N^*_i\mu_{i,\mathrm{el}}/kT\right)\int\exp(-[U_{\mathrm{tot}}-U]/kT)\,\mathrm{d}\mathbf{r}_{N_+}\,\mathrm{d}\mathbf{r}_{N_-} \\ &\approx (\Lambda_+)^{-3N^*_+}(\Lambda_-)^{-3N^*_-}\int\exp(-[U_{\mathrm{SR}}/kT)\,\mathrm{d}\mathbf{r}_{N_+}\,\mathrm{d}\mathbf{r}_{N_-}/Q(N^*_+,N^*_+) \\ &= Z^*_{\mathrm{SR}}/Z^* \end{aligned} \tag{45}$$

Z^* is the *configuration integral* for the fixed set of numbers $\{N^*_+, N^*_-\}$ using the *total* interaction energy and Z^*_{SR} is the configuration integral for $\{N^*_+, N^*_-\}$ using only the *short range* interaction energy. Thus, we have in the bulk limit:

$$\ln\langle\exp(U/kT)\rangle_{\mathrm{GCEMC}} \to F^*/kT - F^*_{\mathrm{HS}}/kT \equiv \Delta F(N^*_+, N^*_-)/kT \tag{46}$$

$\Delta F(N^*_+, N^*_-)$ is the *electrostatic Helmholtz' free energy* for the most probable occupation numbers *i.e.* the free energy over and above the hard sphere (HS) free energy with the same occupation numbers in the very large pore.

In hindsight it should be mentioned, that one might also have sampled the following quantity:

$$\left\langle \exp\left(\left[U - \sum N_i \Delta\mu_{i,\mathrm{el}}\right] \Big/ kT\right)\right\rangle_{\mathrm{GCEMC}} = \Xi_{\mathrm{HS}}/\Xi \tag{47}$$

Here

$$\Delta\mu_{i,\mathrm{el}}/kT \equiv (\mu_{i,\mathrm{bulk}}/kT) - z_i\Delta - (\mu_{i,\mathrm{bulk,HS}}/kT) \tag{48}$$

is the difference between the electro-chemical potential in the bulk and the chemical potential in the bulk for a similar electrolyte solution without charge. Since we have in general (also for a small heterogeneous system) that

$$\ln \Xi = (F/kT) + \langle N_+\rangle\mu_{+,\mathrm{el}} + \langle N_-\rangle\mu_{-,\mathrm{el}} \tag{49}$$

we may calculate the excess Helmholtz' free energy for a pore of *finite size* from GCEMC simulations with and without charges on the ions. This will be done in future publications.

In Figure 13 are shown the values of the excess energy divided by the mean number of ions in *uncharged pores* relative to the bulk values $E_{\mathrm{ex}}(\infty)/NkT$ plotted against $1/(\tau\kappa a)$. The bulk values were obtained earlier by canonical ensemble Monte Carlo simulations (CEMC) with periodic boundary conditions using special extrapolations to an infinite system [3, 10, 11, 13]. For small values of $1/(\tau\kappa a)$ – *i.e.* large pores compared to the Debye length – the curves for the different Bjerrum parameters and concentrations seem to follow a common curve, which extrapolate to unity, since the bulk values are obtained in the limit of very large pores. However, individual differences appear for small pores when $1/(\tau\kappa a) > 1$. Probably, the values for $B = 6.8116$ at high dilution are closer to the bulk value because a considerable part of the interionic interaction energy is with the contact adsorbed counterions on the ions and not in the diffuse ionic cloud. Such ion pairs form easily, when there are at least two ions in the pore, and then it is difficult to separate them again.

The curves of the relative excess energy decrease from unity at $1/(\tau\kappa a) = 0$ to zero at $1/(\tau\kappa a) \to \infty$. The decay seems to be bi-exponential. The initial decrease is of first order in the parameter $1/(\tau\kappa a)$, and it is quite steep. This should be contrasted with CEMC simulations with periodic boundary conditions of period a and minimum image energy cut-off, where $E_{\mathrm{ex}}(L)/\mathrm{E}_{\mathrm{ex}}(\infty)$ deviates from unity with a leading term of the *square* of the corresponding parameter $2/[L\kappa a]$. This shows the advantage of using periodic boundary conditions for the extrapolation of bulk quantities to the thermodynamic limit. In principle GCEMC pore simulations may also be used to extrapolate to bulk properties, but for the same precision one has to use pores with a larger value of $2\langle N\pm\rangle$ than the values of the number of ions N in the CEMC simulation box. For pores, however, the values of the excess energy for finite pores have a physical meaning.

A similar plot is shown for $\ln\langle\exp(U/kT)\rangle/[2kT\langle N\pm\rangle]$ relative to $\Delta F_{\mathrm{ex}}(\infty)/NkT$ in Figure 14. All the pores are without surface charge. The curves seem to extrapolate neatly to the bulk value (unity) for large pores, but the exponen-

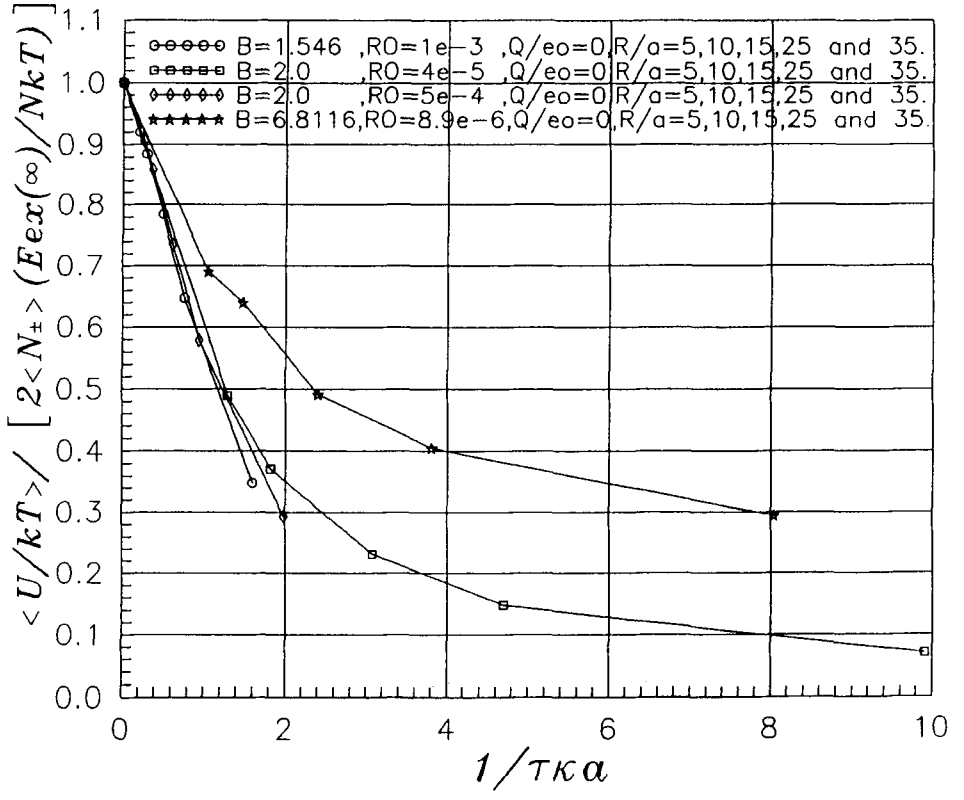

Figure 13 The mean of the electrostatic interaction energy per ion for chargeless pores relative to the excess energy per ion $E_{ex}(\infty)/NkT$ in a bulk electrolyte (CEMC data extrapolated to the thermodynamic limit, see references [10] and [13]). Three different B-values and 4 different ρ^* values are investigated. The fraction of the bulk excess energy is approximately scaled by $1/(\tau\kappa a)$ for not too small pores, but especially the very dilute $B = 6.8116$ electrolyte deviates from the other electrolytes. This electrolyte has strong ion pairing and the excess energy is less affected by the truncation of the ion cloud. For large pores, the ratio extrapolates to unity.

tial decrease is even more steep than for the excess energy. Again, different values of B and κa seem to evolve individually for small pores. In Figure 15, a similar plot for $\mathrm{VAR}(U/kT)/\{2\langle N\pm\rangle\}$ relative to $C_{V,ex}(\infty)/Nk$ is shown. We observe, that the extrapolated value for large pores is definitely larger than unity because of the additional fluctuation term in a grand canonical ensemble.

The surface charge has a great influence on the excess thermodynamic quantities. As an example, we show in Figure 16 the values of the excess energy per ion relative to the extrapolated CEMC value for $B = 1.546$, $\kappa a = 0.139383$ as functions of $1/(\tau\kappa a)$ for $Q/eo = 0$, 1, 5 and 10. All values have been calculated at *Donnan electroneutrality* of the pore. The rise is the more steep the higher is the surface charge. This is due to the interaction between the pore ions and the surface charge as well as the Donnan potential (from the surrounding pores). It should be noticed, that when the relative excess energy is higher than 1, the excess energy per ion in the pore is *more negative* than in the bulk solution. Thus, the ions are greatly

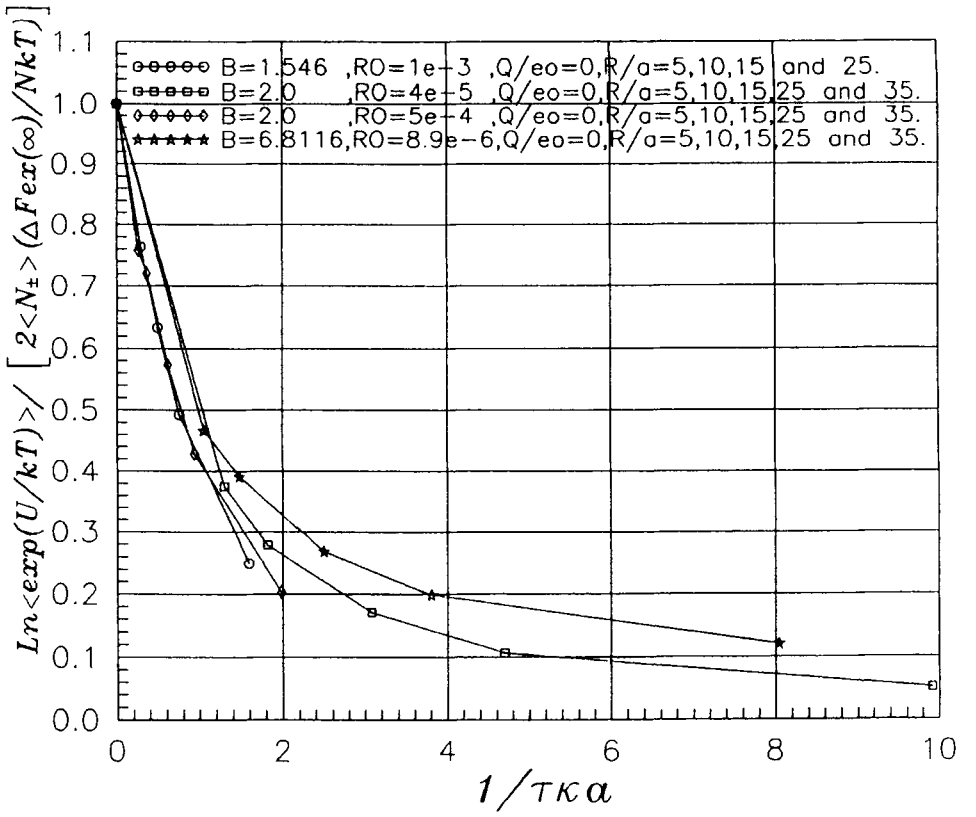

Figure 14 The mean of $\ln\langle\exp(U/kT)\rangle$ per ion for chargeless pores relative to the electrostatic Helmholtz free energy per ion $\Delta F_{ex}(\infty)/NkT$ in a bulk electrolyte (CEMC data extrapolated to the thermodynamic limit, see refs. [10] and [13]). The same electrolytes as in Figure 13. The curves extrapolate to unity for large pores as predicted by the maximum term method, but for finite pores $\ln\langle\exp(U/kT)\rangle$ has no physical meaning. (*A* value with $R/a = 35$ for the $B = 1.546$ and $\rho^* = 0.001$ electrolyte is omitted. The configurational energies are here quite large, and more than 60 million configurations seem to be necessary for convergence of $\langle\exp(U/kT)\rangle$).

stabilized by interaction with the surface charge, since the ions with the same sign of the charge as the surface charge is *Donnan excluded*. The mean interaction energy between the ions themselves become less negative or even positive, but the interaction with the surface charge and with the Donnan potential dominates for small pores.

Finally, we return in Figure 17 to the mean population number $\langle N\pm\rangle$ in uncharged pores. For $B = 2$ we have plotted $\langle N\pm\rangle/\langle N\pm\rangle_{bulk}$ against $1/\tau$ for $\kappa a \approx 0.02242$ and $\kappa a \approx 0.1121$. (Plotting against $1/[\tau\kappa a]$ does not reduce the two curves to a common plot). For large pores, the two curves extrapolate to the bulk value (unity). At the low concentration, it is clearly seen that the curve converges to the value of the *mean activity coefficient in the bulk* when the pores become small. The minimal pore model (appendix B) converges to the same limit at $\tau \to 0$, see Equation (B16). (However, the value of $1/\tau$ has to be greater than 2 for this model to be valid, and the values of $\langle N\pm\rangle/\langle N\pm\rangle_{bulk}$ then converges towards

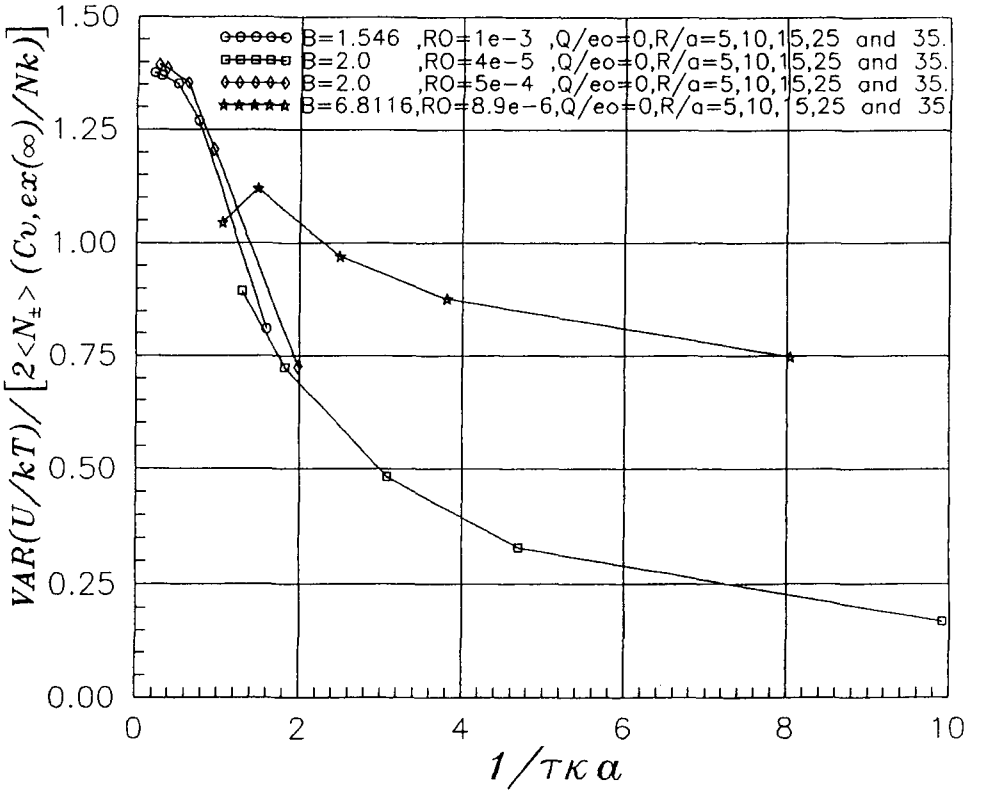

Figure 15 The variance of U/kT per ion for chargeless pores relative to the bulk heat capacity at constant volume per ion $C_{V,ex}(\infty)/Nk$ (CEMC data extrapolated to the thermodynamic limit, see references [10] and [13]). The same electrolytes as in Figure 13. The curves extrapolate to a value greater than unity for large pores due to the fluctuation terms in a grand canonical ensemble. The correction term is complicated, but with this term the depicted values for pores of finite size have a physical meaning. The $B = 6.8116$ electrolyte deviates from the rest, and there seems to be a convergence problem for the value for $R/a = 35$.

$y \pm$ (bulk) from *lower* values!). Similarly, it seems plausible from Figure 17, that $\langle N\pm\rangle/\langle N\pm\rangle_{bulk}$ also approaches $y \pm$ (bulk) corresponding to $\kappa a \approx 0.1121$ for this higher concentration.

In principle, the concentration corresponding to a given chemical potential in bulk solutions may be extrapolated from GCEMC simulations in neutral pores, but once more this method can hardly compete with CEMC test particle sampling with correction to electroneutrality and $2/(L\kappa a)$ extrapolation [10–11].

DISCUSSION AND CONCLUSIONS

We have shown that many interesting features with relevance to microporous media are exhibited from GCEMC simulations of a simple model of charged or uncharged

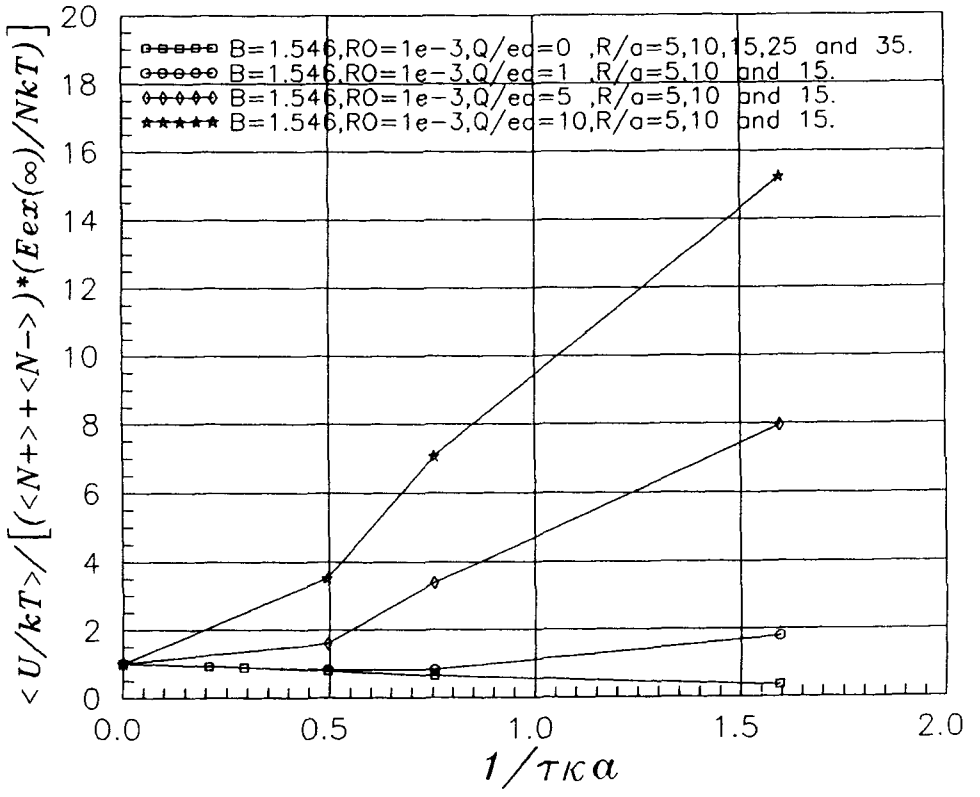

Figure 16 The mean of the electrostatic interaction energy per ion for charged pores relative to the excess energy per ion $E_{ex}(\infty)/NkT$ in a bulk electrolyte. $B = 1.546$ and $\rho^* = 0.001$. Surface charges for the curves from above: $Q/e_0 = 10$, 5, 1 and 0. For large pores ($\tau\kappa a \rightarrow \infty$), all curves tend towards unity.

spherical, hard pores - or rather "alveoles" with hard sphere ions. The following conclusions have been reached:

1) An isolated, charged alveole in equilibrium with an external solution with cations and anions of the same size is *not* electroneutral. On the contrary, it aquires a *spontaneous electrification.* For a given surface charge, this electrification is a function of the radius of the accessible pore volume measured in Debye lengths ($\tau\kappa a$), see Figures 1-2. The decay of the spontaneous electrification with $\tau\kappa a$ towards zero seems approximately exponential. In all cases, positively charged pores obtain a positive spontaneous electrification. The electrification varies from the surface charge for very small pores (or for very small concentrations $\sim \kappa$) to zero for very large pores (or large concentrations). This is true for very dilute to moderately concentrated salt solutions and a number of Bjerrum parameters. However, for a very dilute electrolyte with high Bjerrum parameter (≈ 6.8) there is some deviation from the "universal" scaling in very small pores with high surface charge. In this case, the electrification is less than expected, which might well be a result of a strongly bound

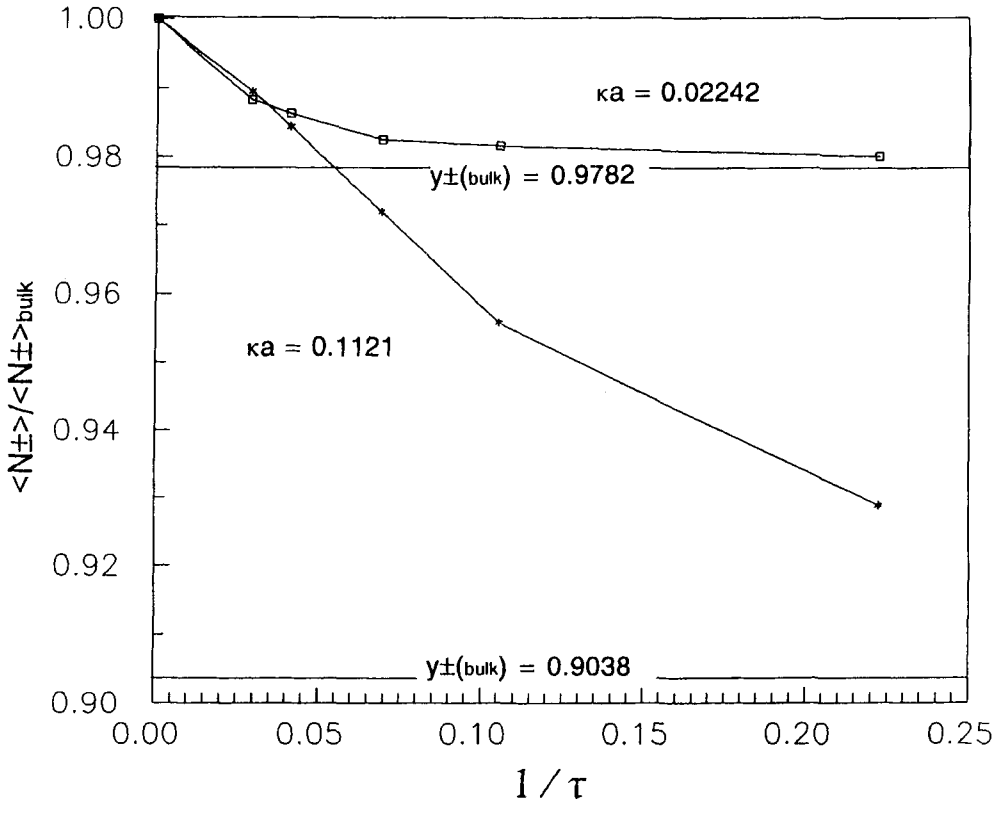

Figure 17 The geometric mean of the population numbers in the pores divided by the corresponding values for the same volume of the bulk electrolyte *vs.* $1/\tau$. $B = 2$ and two different concentrations. The curves run from unity for large pores to $y_{\pm}$(bulk) for small pores.

contact adsorbed surface layer of negative counterions – lowering the effective net surface charge for the diffuse electric double layer.

2) The spontaneous electrification is affected by an external change in the dimensionless *electric potential difference* (Δ) between the alveole and the external solution as well as by the dimensionless electric potential induced by the surface charge (η). The electrification decreases with the dimensionless *total applied potential* ($\zeta = \Delta + \eta$). For higher values of ζ, the electrification of alveoles with a positive surface charge becomes negative. The electrification will be zero for an applied potential $\Delta = \Delta_D$, which is the *Donnan potential* for the alveole. This potential is approximately the potential difference aquired between a very large *membrane phase* with many alveoles of the same size imbedded in an almost ion-free membrane matrix and a surrounding solution in order to prevent any deviation from electroneutrality of the membrane phase. The total applied potential at Donnan equilibrium (ζ_D) increases with the positive surface charge and decreases with increasing alveolar radius, see Figures 3–5. Negative values of Δ may also be applied

to generate values of ζ approaching zero (Figure 6). At zero total applied potential, cations and anions of the same size enter the alveole with equal probability, and the electrification will be equal to the surface charge (Q/e_0) for all pore sizes. Increasing the applied potential from this value results in a decrease in the electrification which is steeper the greater is the pore radius, since it is more difficult to change the ionic balance in small pores because of space restrictions.

3) Performing GCEMC simulations for a number of Δ-values near to the point of the electroneutrality, the *Donnan potentials* for various alveoles and electrolytes were determined with 4 digit precision. For an example, see Figure 7. A general second order equation is derived, which permits the calculation of Δ_D, if the bulk and pore single ion activity coefficients were known, Equation (28). Since this is not the case, the equation is used the other way round: Knowing the Donnan potential - or in fact just the potential Δ - and knowing the ratios between the bulk and pore mean ionic activity coefficients, the ratios between the single ion activity coefficients and the mean ionic activity coefficients in the pore may be calculated, see Equation (30) and conclusion 5 below. When all activity coefficient ratios are put equal to zero, Equation (28) simplifies to the usual Donnan polynomial for calculating the *ideal Donnan potential* Δ_D (ideal), Equation (29). In very dilute systems and for low surface charges, the Donnan potentials simulated are very close to the ideal Donnan potentials. At higher concentrations and at higher surface charges, the deviations may be appreciable. It is interesting to notice, however, that the small pores generally have Donnan potentials with the least deviations from the ideal values. The Donnan potentials and their percentage deviations from the ideal values are collected in Table 4.

4) The mean *ionic occupation numbers* in the alveoles $\langle N\pm \rangle$ are found from the GCEMC simulations. The corresponding value for one alveolar accessible volume taken from the bulk solution is $\langle N\pm \rangle_{bulk}$. The ratio between $\langle N\pm \rangle$ and $\langle N\pm \rangle_{bulk}$ depends solely on the total applied potential (ζ) for the same electrolyte and the same pore size (Figure 8). The mean ionic occupation numbers always increase with increasing total applied potential, which is briefly called *electrosorption*. The increase is less for large pores than for small ones. In bulk solution any applied potential has no consequence for $\langle N\pm \rangle_{bulk}$.

5) The *average mean ionic* and the *average single ionic activity coefficients* for the ions in the alveoles may be calculated from $\langle N\pm \rangle/\langle N\pm \rangle_{bulk}$ and from the non-ideal Donnan polynomial, see conclusion 3 above. The values of the activity coefficients at the Donnan potential (for uncharged pores at $\Delta = 0$) are tabulated in Table 5. The most important conclusion is, that *average pore activity coefficients in finite phases are dependent on the applied electric potential.* The mean ionic activity coefficient decreases somewhat with increasing potential (electrosorption, Figure 9) and the single ion activity coefficients in the alveole are extremely potential sensitive (Figures 10–12). Thus, the usual division of the electrochemical potential

$$\mu_{el,i} = \mu^0{}_i + kT \ln (y_i \rho_i / \rho^0{}_i) + z_i e_0 \Psi \tag{32}$$

is presented in a new light. The division into a "chemical" part and an "electric" part is all right, but the chemical part is also dependent on the electric potential in phases of finite extension. It is of course arbitrary, whether the potential dependence is ascribed to the activity coefficient or to the standard potential. In this paper we have chosen the same standard state in the accessible part of the pore as in the exterior solution, and the potential dependence is delegated to y_i. The

potential dependence of the chemical part of the electrochemical potential is likely to be found also in more realistic models of ion exchange membranes, and will be of fundamental significance for their description. As an example, the separation in traditional irreversible thermodynamics into the driving forces $-\nabla\Psi$ and $-\nabla\mu_i$ is less clear cut in strong ion exchange membranes!

6) The results for the GCEMC simulations with a given B are stated here as for 1:1 electrolytes. A high value of B may mean either a 1:1 electrolyte at low dielectric constant or a z:z electrolyte at the dielectric constant of water. The restricted primitive model does not distinguish between these cases for bulk electrolytes. In the pores, however, it is important to know the valency of the electrolyte to calculate the electrification. However, the GCEMC calculations which have been performed as if they were for 1:1 electrolytes may always be interpreted as simulations for z:z electrolytes, if we multiply the tabulated surface charges by z and divide the tabulated values of the applied potential by z. This is what is called *z-invariance.*

7) The *excess energy per ion* in *alveoles without charge* is a fraction of the similar values in the bulk phase found by proper extrapolation of CEMC data. This fraction may be plotted against $1/(\tau\kappa a)$ and the plots are approximately bi-exponential decaying from unity at $1/(\tau\kappa a) = 0$ (infinite large pores) to zero at infinitely small pores (Figure 13). For small values of $1/(\tau\kappa a)$ the simulation values seem to follow a common curve without regard to B and κa, but for $1/(\tau\kappa a) > 1$ the curves spread out individually. Especially the curve for $B \approx 6.8$ shows a much smaller decrease in the relative energy than the ones for the lower B-values. This might well be a result of the strong ion pairing and the significant contribution from such interactions compared to the ionic cloud interactions. Close ion pairs are disturbed only to a small degree by the space restrictions in small pores. The excess energy in alveoles with *non-zero surface charge* is of course deeply affected by the interaction with the surface charge as well as by the Donnan exclusion of co-ions to the surface charge. These effects act in opposite directions, but the first effect dominates (Figure 16).

8) Similar plots may be made for the values of $\langle \exp(U/kT) \rangle$ in pores without charge. In the limit of large pores this quantity extrapolates to the *excess electrostatic Helmholtz free energy per ion* for the ions in the bulk (Figure 14).

9) The *variance* of U/kT may be treated similarly, but the values are *higher* than the excess heat capacity at constant volume in the pores because of additional fluctuation terms in a grand canonical ensemble (Figure 15).

10) The relative mean population numbers $\langle N\pm \rangle / \langle N\pm \rangle_{\text{bulk}}$ seems to extrapolate smoothly to unity at $1/\tau = 0$, see Figure 17. For $\tau \to 0$, the limiting value is $y\pm$ (bulk) - a value predicted also by the minimal pore model, see conclusion 11.

11) To find *bulk values* of the electrolyte properties (excess energy, excess electrostatic Helmholtz' free energy and ion density) one might perform GCEMC simulations with the excess chemical potential as input in non-charged alveoles at increasing size. However, the first correction term for finite system size is of *first order* in $1/(\tau\kappa a)$ and the dependence is quite strong. In contrast, the first correction term in the case of CEMC simulation with periodic boundary conditions (period L scaled by the ion diameter) and minimum image energy cut-off is of *second order* in $2/(L\kappa a)$. Therefore, this kind of GCEMC simulation is no real alternative to CEMC simulations with varying period. (GCEMC simulations with periodic boundary conditions is all right, of course).

12) For very small alveoles ($\tau < 0.5$), there may only be one ion at a time in the alveole, and there are therefore only three potential energy states in the model. The

grand canonical partition function may then be evaluated *analytically*. This model is called the *minimal pore model* and some consequences of this model are stated in the appendix B. It has certain similarities to the general model (z-invariance, spontaneous electrification, dependence of the electrification on the total electric potential and potential dependent activity coefficients), but is also strikingly different (κ has never any importance, Donnan potentials do not always exist). It acts in certain respects as a limit of the general model (the relative mean ionic population number being $y \pm$ (bulk) in very small alveoles, for example). In other respects, there is a clear jump in properties for $\tau = 0.5$, for below this value the *diffuse double layer has no meaning*. For pores above this value, we have seen in this paper and in Reference [1], that many properties are dominated by the *Debye length*, even if the average population number of ions are only a tiny fraction of a whole ion. The important thing is, that there *some times* are two (or more) ions in the pore!

In a forthcoming paper, we shall discuss the influence of having two different sizes of the ions, and we shall also discuss in details the ion distribution functions and the electric potential distribution in the alveoles. The case with two dielectric constants (one for the pore, another for the wall) is of great interest, but the expression for the configuration energy is very involved, since a generalisation of the image charge concept to spherical geometry does not exist. Thus, such simulations will have long calculation times, but we are proceeding with these calculations and we hope to state the first results in a still later publication.

Acknowledgement

We are grateful to Prof. Niels Bjerrum, Chemical Laboratory A, Technical University of Denmark, for his support at a critical stage during the completion of this work.

APPENDIX A

METHODOLOGY AND BASIC NOMENCLATURE

The system is described by the occupation numbers N_+ and N_- for the cations and the anions, which are at positions $\mathbf{r}_{N_+}$ and $\mathbf{r}_{N_-}$. The semi-classical probability density of having such a state in a grand canonical ensemble with cations and anions being indistinguishable between themselves is given by:

$$P(N_+, N_-, \mathbf{r}_{N_+}, \mathbf{r}_{N_-})\, d\mathbf{r}_{N_+}\, d\mathbf{r}_{N_-} =$$

$$(\Lambda_+)^{-3N_+}(\Lambda_-)^{-3N_-}\Xi^{-1}\exp(\beta[N_+\mu_{+,\mathrm{el}} + N_-\mu_{-,\mathrm{el}} - U(\mathbf{r}_{N_+}, \mathbf{r}_{N_-})])\, d\mathbf{r}_{N_+}\, d\mathbf{r}_{N_-} \quad \text{(A1)}$$

where Λ_+ is the thermal deBroglie wavelength for the cation, Ξ the grand canonical partition function $\beta = 1/kT$, $\mu_{-,\mathrm{el}}$ the electrochemical potential for the anion and U the configurational energy. We consider a Markov process between states i and j with transition probability p_{ij}:

$$\{N_+^{(i)}, N_-^{(i)}, \mathbf{r}_{N_+}^{(i)}, \mathbf{r}_{N_-}^{(i)}\} \underset{p_{ij}}{\rightarrow} \{N_+^{(j)}, N_-^{(j)}, \mathbf{r}_{N_+}^{(j)}, \mathbf{r}_{N_-}^{(j)}\} \quad \text{(A2)}$$

Because of *microscopic reversibility* we need to have:

$$p_{ij}P_i\, d\mathbf{r}_{N_+}^{(i)}\, d\mathbf{r}_{N_-}^{(i)} = p_{ji}P_j\, d\mathbf{r}_{N_+}^{(j)}\, d\mathbf{r}_{N_-}^{(j)} \quad \text{(A3)}$$

The transition probabilities satisfy the constraints:

$$\sum_j p_{ij} = 1 \quad \text{(for all } i\text{)} \tag{A4}$$

We break down the transition probabilities into two probabilities

$$p_{ij} = q_{ij} f_{ij} \tag{A5}$$

where q_{ij} is the probability of *attempting* a move and f_{ij} the probability of *acceptance* of the given move. From equations (A3) and (A5) we obtain:

$$q_{ij} f_{ij} P_i \, \mathrm{d}\mathbf{r}_{N_+}{}^{(i)} \, \mathrm{d}\mathbf{r}_{N_-}{}^{(i)} = q_{ji} f_{ji} P_j \, \mathrm{d}\mathbf{r}_{N_+}{}^{(j)} \, \mathrm{d}\mathbf{r}_{N_-}{}^{(j)} \tag{A6}$$

We consider four types of moves each with a probability = 1/4:

1) Addition of a cation to a random position
2) Addition of an anion to a random position
3) Removal of a randomly chosen cation
4) Removal of a randomly chosen anion

(A7)

For example, a process of type 1 may be written

$$\{N_+{}^{(i)}, N_-{}^{(i)}, \mathbf{r}_{N_+(i)}, \mathbf{r}_{N_-(i)}\} \underset{p_{ij}}{\rightarrow} \{N_+{}^{(i)} + 1, N_-{}^{(i)}, \mathbf{r}_{N_+(i)}, \oplus\, \mathbf{r}_{N_+(i)+1}, \mathbf{r}_{N_-(i)}\} \tag{A8}$$

whereas process 3 is just the reverse. Thus we see, that the attempt probabilities of the processes 1 and 2 are given as

$$q_{\text{addition}} = (1/4)\,(\mathrm{d}\mathbf{r}_{\text{new ion}}/V_{\text{type of ion}}) \tag{A9}$$

where $V_{\text{type of ion}}$ is the accessible portion of the spherical pore for the given type of ion. (NB! In the earlier version of the programme described in Reference [1], the volume was here put equal to the total volume of the sphere, and for every insertion of a new ion it was tested, if there were overlap with the wall. If overlap, the move was rejected and the previous move was counted once more. The result is the same, but the present procedure saves time, since we have not to test for wall overlap).

For the processes 3 and 4 we have:

$$q_{\text{removal}} = (1/4)\,(1/[N^{(i)}{}_{\text{type of ion}} + 1]) \tag{A10}$$

No processes involving displacements of ions within the systems need to be considered, since all configurations and occupation numbers may be generated by the four processes (A7). Taking the process ij to be an addition process, we have from equations (A6), (A8), (A9) and (A10):

$$P^{(i)}{}_{\text{ion not added}}/P^{(j)}{}_{\text{ion added}} = (V_{\text{type}}/[N^{(i)}{}_{\text{type}} + 1])\,(f_{\text{removal}}/f_{\text{addition}}) \tag{A11}$$

Using Equation (A1) we find:

$$P^{(i)}{}_{\text{ion not added}}/P^{(j)}{}_{\text{ion added}} = (\Lambda_{\text{type}})^3 \exp(-\beta\mu_{\text{type,el}}) \exp(+\beta\Delta U) \tag{A12}$$

$$\Delta U \equiv U^{(j)}{}_{\text{ion added}} - U^{(i)}{}_{\text{ion not added}} \tag{A13}$$

From equations (A11) and (A12) it follows that:

$$(f_{\text{rem}}/f_{\text{add}}) = [N^{(i)}{}_{\text{type}} + 1]\,(\Lambda^3{}_{\text{type}}/V_{\text{type}})\exp(-\beta\mu_{\text{type, el}})\exp(+\beta\Delta U) \quad \text{(A14)}$$

For the electrochemical potential of an ion we write:

$$\mu_{\text{type, el}} = \mu_{\text{type}}(\text{chemical, bulk}) + q_{\text{type}}\Psi_b \quad \text{(A15)}$$

where q_{type} is the charge of the ion added or removed ion and Ψ_b the electric potential in the bulk phase. We may introduce the excess chemical potential μ_{type} (ex) and the (absolute) single ion activity Z_{type} (dimension volume^{-1}):

$$\beta\mu_{\text{type}}(\text{chemical, bulk}) = \ln[\Lambda^3{}_{\text{type}}Z_{\text{type}}] = \beta[\mu_{\text{type}}(\text{ideal}) + \mu_{\text{type}}(\text{ex})] \quad \text{(A16)}$$

$$\beta\mu_{\text{type}}(\text{ex}) = \ln[Z_{\text{type}}/\rho_{\text{type}}] \quad \text{(A17)}$$

$$\beta\mu_{\text{type}}(\text{ideal}) = \ln[\Lambda^3{}_{\text{type}}\rho_{\text{type}}] \quad \text{(A18)}$$

In equations (A17) and (A18), ρ_{type} is the bulk density of the ion type which is added or removed. Equation (A14) may be written as:

$$(f_{\text{rem}}/f_{\text{add}}) = [(N_{\text{type, after addition}}/[V_{\text{type}}\cdot Z_{\text{type}}])\exp(+\beta(\Delta U - q_{\text{type}}\Psi_b))] \quad \text{(A19)}$$

If the electric potential from *external fields* at the insertion point is Ψ_{in} we have

$$\Delta U = \Delta U^* + q_{\text{type}}\Psi_{\text{in}} \quad \text{(A20)}$$

where ΔU^* is the change in configurational energy *from pair interactions alone.* Thus we have:

$$(f_{\text{add}}/f_{\text{rem}}) = (V_{\text{type}}\cdot Z_{\text{type}}/N_{\text{type, after addition}})\exp(\beta q_{\text{type}}\Psi_b)\exp(-\beta\Delta U^* - \beta q_{\text{type}}\Psi_{\text{in}}) \quad \text{(A21)}$$

We write

$$(f_{\text{add}}/f_{\text{rem}}) = \text{function}(\Delta U^*, \Psi_{\text{in}}) \quad \text{(A22)}$$

and adopt the following convention: If we have chosen addition and if function > 1, we accept the move ($f_{\text{add}} = 1$). Otherwise (function $\leqslant 1$), we put $f_{\text{add}} = \text{function}$. If removal has been chosen, and if function $\geqslant 1$ (the function for the inverse addition process), we put $f_{\text{rem}} = 1/\text{function} \leqslant 1$. Otherwise (function < 1), $f_{\text{rem}} = 1$ (removal accepted). Playing this game for a while, we obtain a stochastic equilibrium, where the relative probabilities are distributed as in a grand canonical ensemble, so sampling various properties over the Markov chain (like the ion distributions over the spherical shells of the pore, the occupation numbers, the interaction energy) will ultimately lead to the exact thermodynamic mean values.

It is important to note here, that knowledge of *bulk single ion activities* – unmeasurable by standard electrochemical methods – is necessary for the above calculations. That is, the distribution of ions in pores and the thermodynamic properties of the pore ions are dependent on the thermodynamic properties of single ions in the external solution. In statistical mechanics, single ion activities may be calculated, when the Hamiltonian is known, by various methods. Very recently, it has been shown, how the test particle method introduced by Widom [7, 8] may be

used to find single ion activities in primitive model electrolytes after certain analytical methods of correcting to electroneutrality have been applied [3, 10, 11]. In the present paper, however, we treat only restricted primitive model electrolytes (two ions with the same absolute charge and the same size), so single ion activities and mean ionic activities are identical. The mean ionic activity coefficients for the dilute systems with $B = 1.546$, 2 and 6.8116 have been found by the corrected Widom Monte Carlo method. The mean ionic activity coefficients for $B = 1.681$ at two higher concentrations have been calculated by precision HNC (hypernetted chain) calculations [9].

We have extended the programme described in Reference [1] to calculate also the dimensionless excess energy:

$$E_{ex}/kT = \langle U/kT \rangle \tag{A23}$$

where U is the configuration energy between the pore ions mutually and between the pore ions and the surface charge Q and $\langle\ \rangle$ means averaging over a grand canonical ensemble or - equivalently - sampling over the Markov process put forward in this appendix. For a RPM $z{:}z$ electrolyte we have (cf. Equation (16) in the main text):

$$U/kT = \sum_i \sum_{j<i} (\pm) B/t_{ij} + \sum_i (\pm) z e_0 (B/z)(Q/e_0)/[\tau + 1/2] \tag{A24}$$

with the Bjerrum parameter given by Equation (11) in the main text and the sums running over all ions present in the pore at the given moment. The dimensionless ion separations (scaled by the ion diameter $= a$) are given as:

$$t_{ij} = r_{ij}/a \tag{A25}$$

The variance of the individual energy samplings has been obtained by sampling also $[U/kT]^2$ and calculating:

$$\mathrm{VAR}(U/kT) = \langle [U/kT]^2 \rangle - \langle [U/kT] \rangle^2 \tag{A26}$$

In the new version of the programme, a number of configurations (typically 30,000) are grouped into samplings with given mean values as in the old version, but a new feature is that a number of samplings (for example 100) are again grouped into supersamplings. The configurations are "forgotten" when a sampling average has been performed, and the samplings are similarly "forgotten" when a supersampling average has been performed. In this way a huge number of configurations may be performed, but remembered is only relatively few supersampling averages. From these averages final mean values and variances may also be performed. When the variance of U/kT calculated from supersampling averages are multiplied by the number of configurations in the supersampling, we obtain another value of $\mathrm{VAR}(U/kT)$ which is statistically identical to the one calculated directly (for a sufficient number of supersamplings). The value of $\mathrm{VAR}(U/kT)$ is also equal to the *excess heat capacity* at constant volume plus an additional - quite complicated number fluctuation term, which does not die out for large pores, see equations (37) and (42-43) in the main text.

Another quantity sampled in the new version of the programme is $\langle \exp(U/kT) \rangle$. When this quantity is sampled over alveoles without charge, we obtain in the

limit of very large pores the exponential of the Helmholtz free energy of a corresponding bulk solution, see equations (45-46).

APPENDIX B

CARRICATURE ANALYTICAL MODEL FOR MINIMAL SPHERICAL PORES

Minimal pores are pores, which are so small that there can only be one ion in the pore. For ions of the same diameter (a), we then have $0.5 + \delta < (R/a) < 1.0$ (or $0 + \delta < \tau < 0.5$), where δ is large enough for the radius of the accessible sphere (τ) to be much greater than the thermal deBroglie wavelengths of the ions. For such a carricature model, the grand canonical partition function (Ξ) can be found analytically. It has some value as a limiting case.

There may be *zero ions, one cation or one anion* in the pore. We obtain

$$\Xi = 1 + V(\Lambda_+)^{-3} \exp(\mu_{+,el}/kT) \exp(-z_+\eta) + V(\Lambda_-)^{-3} \exp(\mu_{-,el}/kT) \exp(-z_-\eta) \tag{B1}$$

with the dimensionless energy

$$\eta = (Q/e_0)\mathbf{B}_r(a/R) \tag{B2}$$

We have for the mean population numbers in the usual way:

$$\langle N_+ \rangle = kT[\partial \ln \Xi/\partial \mu_+]_{V,T,\mu_-,el} \tag{B3}$$

$$\langle N_- \rangle = kT[\partial \ln \Xi/\partial \mu_-]_{V,T,\mu_+,el} \tag{B4}$$

Thus, for the present model

$$\langle N_+ \rangle = V(\Lambda_+)^{-3} \exp(\mu_{+,el}/kT) \exp(-z_+\eta)/\Xi \tag{B5}$$

$$\langle N_- \rangle = V(\Lambda_-)^{-3} \exp(\mu_{-,el}/kT) \exp(-z_-\eta)/\Xi \tag{B6}$$

We perform the transformation

$$V/(\Lambda_i^3) = \langle N_i \rangle_{bulk}/(\rho_i \Lambda_i^3) = (4\pi/3)\tau^3 \rho^*_i \exp(-\mu_i(\text{ideal})/kT) \tag{B7}$$

and since the single ion bulk electrochemical potential is given by

$$\mu_{i,el}/kT = \mu_i(\text{ideal})/kT + \ln y_i - z_i\Delta \tag{B8}$$

we have from Equations (B5-B6):

$$\langle N_+ \rangle = (4\pi/3)\tau^3 y_+ \rho^*_+ \exp(-z_+[\eta + \Delta])/\Xi \tag{B9}$$

$$\langle N_- \rangle = (4\pi/3)\tau^3 y_- \rho^*_- \exp(-z_-[\eta + \Delta])/\Xi \tag{B10}$$

$$\Xi = 1 + (4\pi/3)\tau^3\{y_+\rho^*_+ \exp(-z_+[\eta + \Delta]) + y_-\rho^*_- \exp(-z_-[\eta + \Delta])\} \tag{B11}$$

For a $z{:}z$ electrolyte:

$$\langle N_+ \rangle = (2\pi/3)\tau^3 y_\pm \rho^* \exp(-z\zeta)/[1 + (4\pi/3)\tau^3 y_\pm \rho^* \cosh(z\zeta)] \tag{B12}$$

$$\langle N_- \rangle = (2\pi/3)\tau^3 y_\pm \rho^* \exp(+z\zeta)/[1 + (4\pi/3)\tau^3 y_\pm \rho^* \cosh(z\zeta)] \tag{B13}$$

$$\text{Dimensionless total applied potential} = \zeta = \eta + \Delta \tag{B14}$$

We see that the occupation numbers are functions of z times the total applied potential (ζ) and the bulk mean ionic activity coefficients. Since $z\zeta = (Q/e_0)(\mathbf{B}/z)(a/R) + z\Delta$, we get the same results as for a 1:1 electrolyte, if we multiply the surface charge by z and divide the external potential by z, *i.e.* we have *z-invariance.*

When $\zeta = 0$, $\langle N_+ \rangle = \langle N_- \rangle = (2\pi/3)\tau^3 y_\pm \rho^* / [1 + (4\pi/3)\tau^3 y_\pm \rho^*]$. If we further take the high concentration limit $\rho^* \to \infty$, we obtain $\langle N_+ \rangle = \langle N_- \rangle = 1/2$. Then, all pores are filled up and there is equal probability of having a cation and an anion. In the other limit $\rho^* \to 0$, we have $\langle N_+ \rangle = \langle N_- \rangle = 0$, which is also to be expected.

When $\zeta \to +\infty$, we have $\langle N_+ \rangle \to 0_+$ and $\langle N_- \rangle \to 1_-$, so all pores become filled with anions as expected. The situation is of course symmetric for the cations, when $\zeta \to -\infty$. For the *electrification* of the pore, we obtain:

$$\langle \mathrm{EL} \rangle = (Q/e_0) - z(4\pi/3)\tau^3 y_\pm \rho^* \sinh(z\zeta) / [1 + (4\pi/3)\tau^3 y_\pm \rho^* \cosh(z\zeta)] \tag{B15}$$

The electrification take values between Q/e_0 for $\zeta = 0$ and $Q/e_0 - z$ for $\zeta \to +\infty$ and $Q/e_0 + z$ for $\zeta \to -\infty$. Therefore, the absolute value of the surface charge has to be *less* than z in order that a Donnan potential - where $\langle \mathrm{EL} \rangle = 0$ - is possible at all! For example, with $z = 2$ and $Q/e_0 = 1$, there will be a Donnan potential $\Delta_D = \zeta - \eta$ corresponding to a value of $\zeta > 0$ where $\langle N_- \rangle - \langle N_+ \rangle = 0.5$. However, for $z = 1$, $\langle N_- \rangle - \langle N_+ \rangle$ has to be $=1$ and this is only possible at infinite ζ. In the latter case, we may conclude either that a large phase with a lot of small pores would disintegrate, or that all the pores have to be filled with anions. These anions would be mobile inside the small pores, but they could never escape to a surrounding salt solution unless they are interchanged with another ion of the same or of a different kind. (An exception would be ions in pores very near to the surface, which would escape to a small extent to create a certain surface potential). Considerations of this kind would be close to the reality in some zeolithe minerals used as molecular sieves.

The *spontaneous electrification* is given by Eqn. (B15) with ζ replaced by η. It should be noticed that no scaling with $\tau\kappa a = \tau\sqrt{(4\pi \mathbf{B}\rho^*)}$ independent of the individual values of τ, $\mathbf{B}$ and ρ^* is possible here. This is so since the Debye length (and the electric double layer) has no meaning in a model, where a pore can only be occupied by one ion at a time!

For the *mean ionic occupation number* and the *average mean ionic activity coefficient* in the pore we obtain:

$$\langle N_\pm \rangle = \sqrt{(\langle N_+ \rangle \langle N_- \rangle)} = (2\pi/3)\tau^3 y_\pm \rho^* / [1 + (4\pi/3)\tau^3 y_\pm \rho^* \cosh(z\zeta)] \tag{B16}$$

$$y_\pm(\text{pore}) = y_\pm \langle N_\pm \rangle_{\text{bulk}} / \langle N_\pm \rangle_{\text{pore}} = 1 + (4\pi/3)\tau^3 y_\pm \rho^* \cosh(z\zeta) \tag{B17}$$

The value of $\langle N_\pm \rangle$ *decreases* towards zero for increasing total potential ζ, because $\langle N_- \rangle$ approaches the finite value 1, whereas $\langle N_+ \rangle$ approaches zero. This is in contrast to the electrosorption phenomenon found for pores, where more than one ion may enter.

At $\zeta = 0$, we have $y_\pm(\text{pore}) = 1 + (4\pi/3)\tau^3 y_\pm \rho^*$. In the case of $\rho^* \to 0$, pore ideality is obtained, whereas for $\rho^* \to \infty$ we have $y_\pm(\text{pore}) \to \infty$. This is so, since all pores become filled up with cations and anions with equal probability, and any

further introduction of ions in the pores becomes prohibitive. For $\zeta = 0$, $y_{\pm}$(pore) varies from a little more than one for the smallest pore to a little less than $1 + (\pi/6)y_{\pm}\rho^*$ for the largest (minimal) pore.

For $\zeta \to \infty$ we have that $y_{\pm}(\text{pore}) \to \infty$. Now, because all the pores are filled with anions and the introduction of further ions becomes prohibitive. For large applied potentials we have

$$\mu_{\pm}(\text{excess, pore})/kT = \ln y_{\pm}(\text{pore}) \approx \ln\left([2\pi/3]\tau^3 y_{\pm}\rho^*\right) + z\zeta \qquad \text{(B18)}$$

The values of y_+(pore) and y_-(pore) may also easily be found in this model, if desired.

References

[1] T.S. Sørensen and P. Sloth, "Ion and potential distributions in charged and non-charged primitive spherical pores in equilibrium with primitive electrolyte solution calculated by grand canonical ensemble Monte Carlo simulation: Comparison with generalized Debye-Hückel and Donnan theory", *J. Chem. Soc. Faraday Trans*, **88**, 571 (1992).

[2] B. Malmgren-Hansen, T.S. Sørensen, B. Jensen and M. Hennenberg, "Electric impedance of cellulose acetate membranes and a composite membrane at different salt concentrations", *J. Colloid Int. Sci.*, **130**, 359 (1989).

[3] T.S. Sørensen, "Ions in solution and in weak ion exchange membranes" in *Capillarity Today. Lecture Notes in Physics, Vol.* 386, G. Pétré and A. Sanfeld, eds., Springer-Verlag Berlin-Heidelberg-New York-London-Paris-Tokyo-Hong Kong-Barcelona-Budapest, 1991 pp. 164–221.

[4] T.S. Sørensen, B. Malmgren-Hansen and B. Jensen, "Electromotive force and impedance studies of cellulose acetate membranes: Evidence for two binding sites for divalent cations and for an alveolar structure of the skin layer", *Desalination*, **80**, 293 (1991).

[5] F.G. Donnan, "Theorie der Membrangleichgewichte und Membranpotentiale bei Vorhandensein von nicht dialyserenden Elektrolyten. Ein Beitrag zur physikalisch-chemischen Physiologie", *Z. Elektrochemie*, **17**, 572 (1911).

[6] F.G. Donnan, "Die genaue Thermodynamik der Membrangleichgewichte. II", *Z. phys. Chem. Abt. A*, **168**, 369 (1934).

[7] B. Widom, "Some topics in the theory of fluids", *J. Chem. Phys.*, **39**, 2808 (1963).

[8] B. Widom, "Potential-distribution theory and the statistical mechanics of fluids", *J. Phys. Chem.*, **86**, 869 (1982).

[9] P. Sloth and T.S. Sørensen, "Single-ion activity coefficients and structure of ionic fluids. Results for the primitive model of electrolyte solutions", *J. Phys. Chem.*, **94**, 2116 (1990).

[10] T.S. Sørensen, "Error in the Debye-Hückel approximation for dilute primitive model electrolytes with Bjerrum parameters of 2 and *ca.* 6.8 investigated by Monte Carlo Methods: Excess energy, Helmholtz free energy, heat capacity and Widom activity coefficients corrected for neutralising background" *J. Chem. Soc, Faraday Trans.*, **87**, 479 (1991).

[11] T.S. Sørensen, "High precision canonical ensemble Monte Carlo simulations of very dilute primitive $z{:}z$ and $2{:}1$ electrolytes and of moderately concentrated $1{:}1$ electrolyte mixtures", *Molecular Simulation*, **11**, 1 (1993).

[12] T.S. Sørensen, B. Jensen and B. Malmgren-Hansen, "Electrochemical characterization of cellulose acetate membranes. 1. Influence of hydrogen and Calcium ions on the EMF of LiCl concentration cells with a CA-membrane as separator" *J. Non-Equilib. Thermodyn.*, **13**, 57 (1988).

[13] T.S. Sørensen, "How wrong is the Debye-Hückel approximation for dilute primitive model electrolytes with moderate Bjerrum parameter" *J. Chem. Soc, Faraday Trans.*, **86**, 1815 (1990).

[14] T.L. Hill, *Statistical Mechanics. Principles and Selected Applications*, Dover Publications, New York, 1987, Chap. 4, sections 19–20.